COMPLEX FLOWS OF VISCOELASTIC WORMLIKE MICELLE SOLUTIONS

Jonathan P. Rothstein* and Hadi Mohammadigoushki+

* Department of Mechanical and Industrial Engineering, University of Massachusetts, Amherst, MA 01003 USA

⁺Department of Chemical and Biomedical Engineering, FAMU-FSU College of Engineering, Florida State University, Tallahassee, FL 32310 USA

ABSTRACT

Micelles are formed by the self-assembly of surfactants in solutions. Wormlike micelles or living polymers are a particularly interesting fluids because their long flexible cylindrical geometry can lead to entanglement even at relatively low concentrations. The rheological response of the wormlike micelles is similar in many ways to polymer solutions. Entangled wormlike micelles provide a model fluid system in many respects. In semi-dilute solutions, wormlike micelles show remarkably simple rheological behaviour; their linear rheology is best described by a single-element Maxwell model with a single relaxation time. The non-linear rheological and flow response of wormlike micelles has proven to be incredibly rich and complex. Wormlike micelles are easy to prepare and not susceptible to aging or shear mechanical degradation. Beyond semi-dilute concentrations, nematic and/or hexagonal phases can be observed, allowing an additional level of complexity to be dialled in by increasing concentration. In strong, steady-shear flows, some wormlike micelles have been shown to shear band. In uniaxial extensional flows, wormlike micelle solutions demonstrate enormous strain hardening of their extensional viscosity and under large extensional stresses, can break apart. This failure and the resulting morphological changes of the micelles in the flow have been linked to a number of interesting elastic instabilities. These rheological properties have led to the broad use of wormlike micelle solutions in consumer products as rheological modifiers. In this review, we will discuss a wide range of complex flows of wormlike micelle solutions with both shear and extensional flow components. We will discuss how flow geometry, flow strength, micelle concentration and micelle structure affect these complex flows with a particular emphasis on flow stability.

KEYWORDS: Surfactant solutions; Viscoelastic wormlike micelle solutions; Extensional rheology; Shear rheology; Elastic instabilities.

1. INTRODUCTION

A number of recent review articles have been written on the rheology and applications of wormlike micelle solutions [1-8]. In this review, we intend to focus less on the linear viscoelasticity and/or simple shear deformation response of these fluids and more on the complex flows where a combination of shear deformation and extensional flows exists. Such complex flows are found in a number of industries and applications for which wormlike micelle solutions are commonly used.

Surfactants are amphiphilic molecules which have both a bulky hydrophilic head, which is often charged, and a relatively short and slender hydrophobic tail typically consisting of an 8-20 carbon atom chain. Above their critical micelle concentration (CMC), surfactant molecules in water will spontaneously self-assemble into large aggregates known as micelles to minimize the exposure of their tails to water [9-11]. In oil, reverse micelles are formed where instead the head-groups are shielded from the oil [12, 13]. These large aggregates can form into a number of different complex shapes including spherical, wormlike micelles, vesicles and lipid bilayers [14]. The morphology of the aggregates depends on the size of the surfactant head group, the length and number of tails, the charge on the surfactant, the salinity of the solution, temperature, and the flow conditions [9, 14]. Surfactants with a large head group and/or a single short tail tend to form spherical micelles while surfactants with small head groups and/or a single long tail tend to form wormlike micelles. Surfactants with two or more tails tend to form bilayers. The basis for these relatively simple distinctions are clearly described by Isrealachvili [15] using a packing argument based on the relative effective size of the surfactant head and tail groups.

The phase diagram of surfactant solutions that form wormlike micelle solutions can be quite complex [14, 16]. As the concentration of surfactant in solution is increased, a transition is observed from dilute individual micelles, to semi-dilute entangled micelles, to nematic, hexagonal, cubic or other ordered phases at the highest surfactant concentrations. Within the semi-dilute regime, increasing salt concentration can modify the wormlike micelles from linear, to branched and finally to an interconnected network. For a linear wormlike micelle, the shape and area per unit surfactant molecule is optimized at all positions along the backbone except at the endcaps [9]. When a linear micelle breaks, it must pay an energy penalty by forming two new end caps. In this regime, the electrostatic repulsion of the head groups is strong enough that the increased curvature of an endcap, which spreads the head groups apart, is favored over the concave curvature of a branch point which drives the charged head groups of the surfactants closer together. However, as the salt concentration is increased and the head group charges are sufficiently screened, the wormlike micelles can form three-point or four-point junctions. Evidence of the existence of these branched micelles can be seen in cryo-TEM images [17-22].

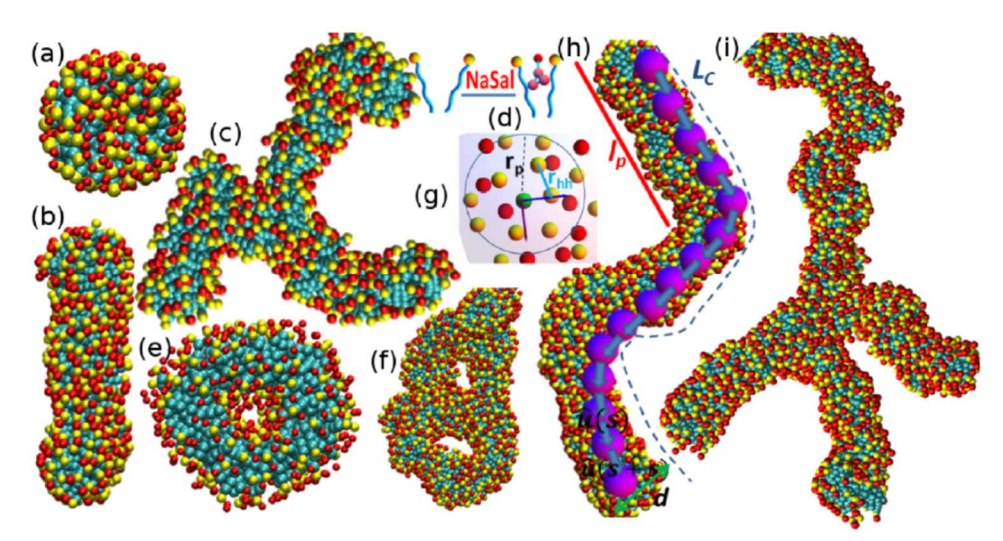


Figure 1: Results from the MD simulations of Dhakal and Sureshkumar [56] showing different possible micelle structures of CTAC/NaSal systems. Of interest here are the molecular structure of the surfactant and salt shown in (d) and the linear and branched wormlike micelles shown in (h) and (i).

This review will focus on surfactants that tend to form either linear or branched wormlike micelles like those shown in Figure 1. At large surfactant concentrations these wormlike micelles can grow very long, become entangled, and make the solution viscoelastic. As suggested by their pseudonym 'living polymers,' wormlike micelles display many of the same viscoelastic properties of polymers. However, although both wormlike micelle solutions and polymer solutions can be viscoelastic, wormlike micelles are physically quite different from polymers. Whereas the backbone of a polymer is covalently bonded, wormlike micelles are held together by relatively weak physical attractions and as a result are continuously breaking and reforming with time. In an entangled network, both individual polymer chains and wormlike micelles can relieve stress through reptation driven by Brownian motion [10]. However, unlike polymeric fluids, wormlike micelle solutions have access to a number of stress relief mechanisms in addition to reptation. Wormlike micelles can relieve stress and eliminate entanglement points by either breaking and reforming in a lower stress state [11] or alternatively by creating a temporary branch point which allows two entangled micelles to pull right through each other thereby eliminating the entanglement point and relieving stress in what has become known as a 'ghost-like' crossing [23].

Viscoelastic wormlike micelle solutions are currently being used extensively as rheological modifiers in consumer products such as paints, detergents, pharmaceuticals, lubricants and emulsifiers where careful control of the fluid properties is required. In addition, micelle solutions have also become important in a wide range of applications including agrochemical spraying, inkjet printing, turbulent drag reduction and enhanced oil recovery where they are often used as a polymer-free fracture fluid for stimulating oil production [1, 2, 24]. In these applications, wormlike micellar solutions experience a combination of shear and extensional deformation. A fundamental understanding of the behaviour of these complex fluids in different flow regimes is therefore extremely important to a host of industries. This has prompted a considerable interest in the complex fluid community to interrogate the flow behaviour of wormlike micelles in simple shear, uniaxial extensions and complex flows where a combination of shear deformation and uniaxial extension exists. The response of the wormlike micelles in shear flows has been extensively studied in the past three decades and multiple reviews have been complied on this topic [4, 8]. However, although, a number of studies of the response of wormlike micelles in uniaxial extensional flows and complex flows have been published over the last two decades, a critical review of such studies is needed. It is the aim of this review to summarize the results of those studies.

The outline of this review is as follows. In section 2, we discuss extensional rheology measurements. In section 3, we discuss flows of wormlike micelle solutions past a falling sphere. In Section 4, we discuss flows of wormlike micelle solutions past a stationary cylinder. In section 5, we discuss flows of wormlike micelle solutions in a range of other complex flows like contraction-expansions, cross-slots and sharp bends. Note that another important example of complex flow is the flow in porous medium. The response of micellar solutions in porous medium has been reviewed in great details in a recent review by Zhao et al [7], and therefore, readers are encouraged to read this recent publication [7]. Finally, in section 6 we conclude and present our outlook for future research in this area.

2. EXTENSIONAL RHEOLOGY OF WORMLIKE MICELLE SOLUTIONS

Over the past thirty years, extensional rheology has become a topic of great interest and importance to the complex fluids community. In particular, the extensional behavior of polymeric fluids has received a considerable amount of attention [25]. However, even though they are less well studied, the behavior of

wormlike micelles solutions in extensional flows has been shown to be incredibly rich and complex. The extensional behavior of wormlike micelle solutions was initially studied using the four roll mill and the opposed jet device [26-33]. Unfortunately, these devices are plagued by an unknown pre-strain history, some degree of shearing in the flow field and the inability to make transient extensional rheology measurements. More recently, the capillary break-up extensional rheometer and the filament stretching rheometer have emerged as accurate devices for reproducibly measuring the response of a wormlike micelle solution to an imposed transient homogeneous uniaxial extensional flow field [34-40]. The results of these techniques will be described in detail here.

2.1 Opposed Jet Device and Four-Roll Mill Measurements and Hyperbolic Contractions

Prud'homme and Warr [26] were the first to perform a comprehensive study of the extensional rheology of wormlike micelle solutions. They studied a series of equimolar tetradecyltrimethylammonium bromide (TTABr) and sodium salicylate (NaSal) solutions in both the dilute and semi-dilute regime using a Rheometrics RFX opposed jet device. In this device, shown schematically in Figure 2(a), two opposed nozzles are immersed in a fluid. Depending on the design, the fluid is then either sucked by a vacuum into

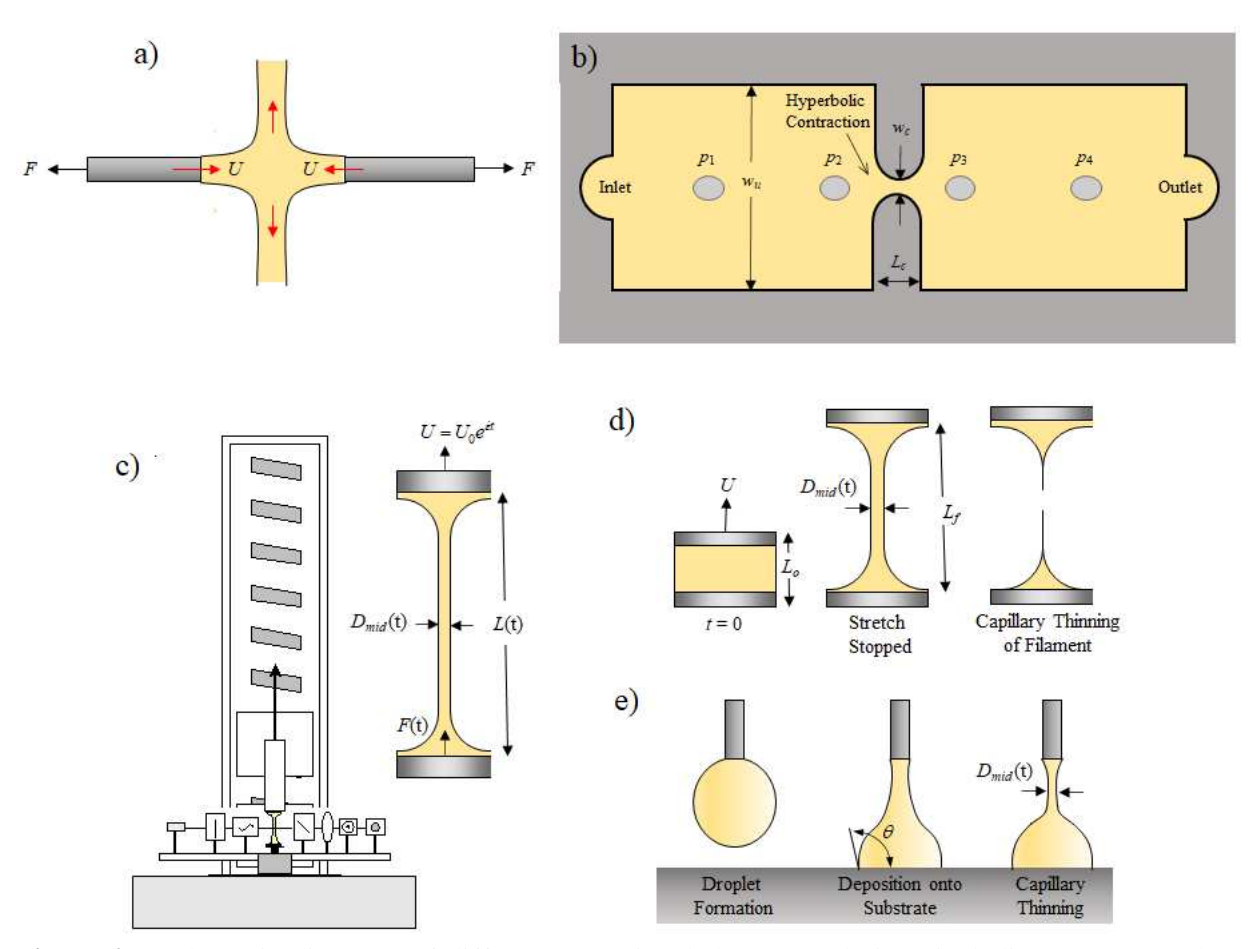


Figure 2: Schematic diagrams of different extensional rheometer designs including: a) Opposed Jet Device, b) microfluidic hyperbolic contraction, c) Filament Stretching Extensional Rheometry (FiSER), d) Capillary Breakup Extensional Rheometry (CaBER), e) Dripping on a Substrate CaBER (CaBER-DoS).

the nozzles or pumped through the nozzle to create two impinging jets. The result is an extensional flow field generated in the small gap between the two nozzles [41]. To calculate the extensional viscosity, the force required to maintain the spacing between the two nozzles is measured.

The response of the wormlike micelle solutions studied by Prud'homme and Warr [26] can be best understood within the framework of polymer reptation theory [10]. At extensional Weissenberg numbers below the coil-stretch transition, $Wi_E = \lambda_E \dot{\varepsilon} < 1/2$, a plateau in the steady-state extensional viscosity was observed corresponding to the Newtonian response, $\eta_E = 3\eta_0$. Here, $\dot{\varepsilon}$ is the extension rate and λ_E is the extensional relaxation time of the fluid. Note that in this review, we will use Wi_E when defining the Weissenberg number based on the extension rate and simply Wi when using the standard definition based off of the shear rate, $Wi = \lambda \dot{\gamma}$. Unlike entangled polymer melts [42], for which tube orientation has been found to result in extension-rate thinning, no such decrease in the steady state extensional viscosity was observed as the Weissenberg number was increased. At higher extension rates, chain stretching within the oriented segments was observed to lead to extensional thickening of the extensional viscosity. At a critical Weissenberg number, the extensional viscosity was observed to reach a maximum and decreases with further increases in Weissenberg number. Unfortunately, the data above this critical Weissenberg number is marred by the onset of a flow instability and the ejection of strongly birefringent fluid from the stagnation region [26]. Even with the problems associated with the stagnation flow field, Prud'homme and Warr [26] theorized that the observed reduction in the extensional viscosity at high extension rates was the result of a scission of the wormlike micelles in the strong extensional flow. The hypothesis of Prud'homme and Warr was later supported by the filament stretching experiments of Rothstein [34]. These results are in qualitative agreement with the results of Walker et al. [30] and Hu et al. [43] who showed a similar dependence of extensional viscosity at large extension rates for a series of cetylpyridinium chloride/sodium chloride (CPyCl/NaCl) and cetyltrimethylammonium bromide/sodium salicylate (CTAB/NaSal) wormlike surfactant solutions respectively in opposed jet devices. Additionally, Walker et al. [30] reversed the flow in the opposed jet device to produce a biaxial extensional flow. The results show a marked difference between uniaxial and biaxial extension with little or no extensional thickening observed for biaxial extensional flows of the wormlike micelle solutions. The latter results suggest that biaxial stretching may be more efficient at disrupting the underlying micelle structure than uniaxial stretching.

In both of these studies, the extensional thickening resulted in Trouton ratios on the order of $Tr = \eta_E / \eta_0 \approx 20 - 40$. Although this is significantly larger than the Newtonian limit of the Trouton ratio which is Tr = 3, for some wormlike micelle systems, Trouton ratios in excess of Tr > 1,000 have been reported [37]. It is therefore important to note that extensional viscosity is a strong function of the choice of surfactant, salt and temperature. For example, Lin et al. [44] used an opposed jet device to measure the extensional viscosity of a number of drag-reducing wormlike micelle solutions. They used a number of oleyl methyl bishydroxyethyl ammonium chloride (O/12) solutions mixed with NaSal at different concentrations and molar ratios. In their study, Trouton ratios exceeding Tr > 500 were found for some samples. A general observation was made that extensional strain hardening decreases with increasing surfactant and salt concentration beyond a molar ratio of 1:1 [44]. These trends were found to be consistent for a number of different surfactant and salt concentrations. In Ober et al. [45], an extensional viscometer rheometer-on-a-chip (EVROC) like that shown in Figure 2(b) was used to measure the extensional viscosity index of a 100mM CPyCl and 60mM NaSal micelle solution and a shampoo, Herbal EssenceTM, containing large amounts of surfactant. From pressure drop measurements across a microfluidic hyperbolic

contraction, the extensional viscosities index of both these solutions were found to thin with increasing extension rates. More recently, Garcia and Saraji [46] provided an improved version of the mathematical estimation of the pressure drop for estimating the apparent extensional viscosity of a range of shear banding and non-shear banding wormlike micellar fluids in the microfluidic hyperbolic contraction geometry.

2.2 Filament Stretching Extensional Rheometry

Although the techniques described in the previous section are capable of measuring an apparent steady-state extensional viscosity of wormlike micelle solutions, the flow fields are inhomogeneous and plagued by an unknown amount of shear. Additionally, they are not capable or making transient measurements. For low viscosity fluids like wormlike micelles, filament stretching extensional rheometers are capable of imposing a transient homogenous extensional flow and measuring extensional viscosity. Filament stretching extensional rheometers (FiSER) like the one shown in Figure 2(c) are often designed with a long linear stage with two sliding motors designed to impose a homogeneous uniaxial extension on a fluid filament placed between its two endplates. While simultaneously measuring the evolution of the midpoint diameter of the fluid filament, this device is capable of measuring the force on one of the endplates and the flow-induced birefringence at the midpoint of the fluid filament [25]. A detailed history of the technique can be found in the following papers by the McKinley and Sridhar groups [25, 47, 48]. The goal of extensional rheometry is to generate a motion profile of the rheometer's endplates such that diameter of the filament is forced to decay exponentially with time and the resulting extension rate imposed on the fluid filament,

$$\dot{\varepsilon} = -\frac{2}{R_{mid}(t)} \frac{dR_{mid}(t)}{dt},\tag{1}$$

is constant. The deformation imposed upon the fluid filament is often described in terms of a Hencky strain, $\varepsilon = -2\ln(R_{mid}/R_0)$, where R_0 is the initial midpoint radius of the fluid filament. The elastic tensile stress difference generated within the filament and thus the extensional viscosity of the fluid is calculated from the total force measured by the load cell affixed to one of the rheometer's endplates [49, 50].

In the work of Rothstein and co-workers [34, 35], a filament stretching rheometer was used to impose a uniaxial extensional flow on a series of CTAB/NaSal and CPyCl/NaSal solutions. Simultaneous measurements of the evolution of the stress and flow induced birefringence (FIB) as a function of time and accumulated strain where made. These fluids were found to demonstrate considerable strain hardening in the elastic tensile stress and extensional viscosity as shown in Figure 3 [34]. Rothstein fitted the extensional response of the wormlike micelle solutions with several different constitutive equations. A good agreement was found between a multimode FENE-P model [51] having a finite extensibility parameter, L^2 , determined from the physical model proposed by Shikata *et al.* [52] which is based on rubber elasticity theory and the knowledge of the wormlike micelle structure derived from light scattering.

As shown in Figure 3(a), above a critical extension rate, the filament stretching experiments of Rothstein and co-workers [34, 35, 53] were observed to come to an abrupt end with the rupture of the fluid filament near its axial midplane. At low Weissenberg numbers, below a critical extension rate, the filaments did not rupture, but instead failed under elasto-capillary thinning as shown in Figure 3(c). A similar break-up phenomenon was observed by Smolka and Belmonte [54] who investigated wormlike micelle solutions

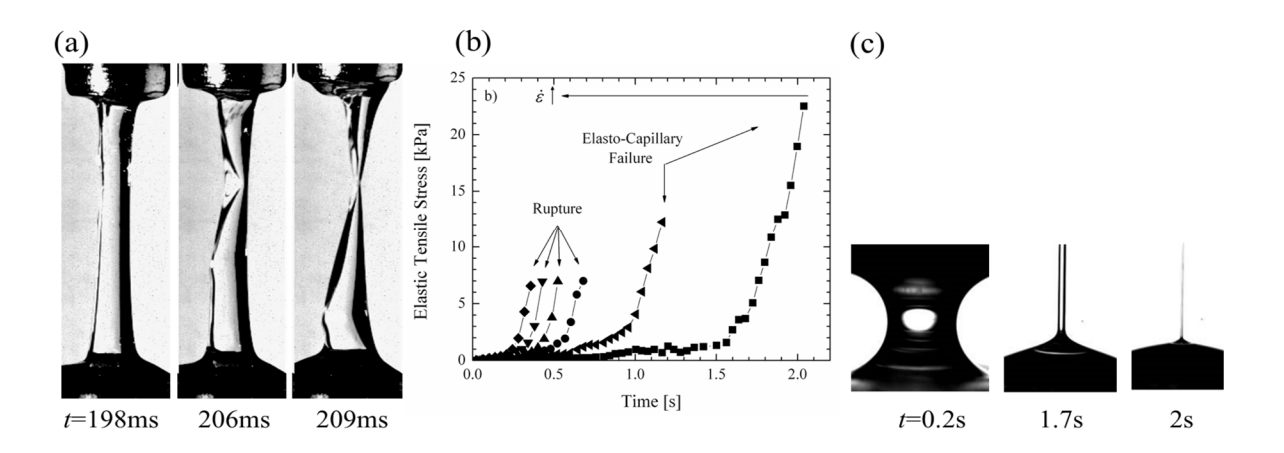


Figure 3: Results from the FiSER measurements of a 150mM/75mM CPCl/NaSal from Bhardwaj et al [35] showing (a) the filament rupture that was observed at Wi_E =2.6, (b) the evolution of the extensional stress as a function of time for a series of increasing Weissenberg numbers from 0.67 < Wi_E < 2.3 and (c) and elastocapillary failure of a filament at Wi_E =0.67.

in a pendant drop experiment. Additionally, Huang and Hassager [55] have recently shown that filaments of stretching polymer solutions can also fracture in a very similar way. In the FiSER measurements, the rupture was found to occur at a constant value of the elastic tensile stress, independent of extension rate. As a result, the calculated value of the extensional viscosity was found to decrease with increasing extension rate, $\eta_{E,max} = \Delta \tau_{nupt} / \dot{\varepsilon} \propto \dot{\varepsilon}^{-1}$. The resulting trends in the extensional viscosity are in qualitative agreement with the extensional rheology measurements performed using an opposed-jet device [26, 30]. It is likely that observed filament failure and the dramatic downturn in the extensional viscosity measured through opposed-jet devices are related and both likely stem from the scission of wormlike micelles resulting in a dramatic breakdown of the micelle network structure *en masse* [34]. At the point of filament failure, the micelles have been heavily stretched and aligned with the flow. The FIB measurements showed nearly-complete elongation of the wormlike micelle with the anisotropy in the wormlike micelle's conformation exceeding 85% of its finite extensibility parameter in all cases, $\Delta A_f > 0.85 L^2$. Additionally, using the tensile stress at rupture, Rothstein estimated the energy barrier for filament rupture and found it to be independent of salt and surfactant concentration [34] for the CTAB/NaSal solutions.

Recent work from the groups of Sureshkumar [56, 57] and of Larson [58] have investigated the dynamics of wormlike micelle solutions in uniaxial extensional flows using coarse-grained molecular dynamics (MD) simulations. Dhakal and Sureshkumar [57] examined the configurational changes to rodlike and bent U-shaped micelles in uniaxial extensional flows. They showed that above a Weissenberg number of $Wi_E > 1/2$, hydrodynamics forces on the micelle were sufficient to straighten out the U-shaped micelle into a rod-like micelle, align it in the flow direction and begin to stretch it. They found that beyond a critical Hencky strain of O(100), the micelles broke in half from a location near mid-point and illustrated that the location of rupture was influenced by the flow-induced depletion of counterions near the midpoint and accumulation of counterions near the ends of the rod-like micelles. More recently, Mandal and Larson [58] used MD simulations to investigate the variation of micelles chain scission energy, breaking stress and the stretch modulus as a function of counterion (hydrotrope) concentration and showed that each displayed a non-monotonic dependence on the ratio of salt to surfactant concentrations, R. The maximum in breaking

stress and the scission energy were shown to occur at $R \sim 0.6$, while the maximum in stretch modulus was found to occur at $R \sim 1.0$ when the micelle was neutrally charged. They compared their simulations results to Rothstein [34] and found good agreement for filament rupture stress once the effects of the very different extension rates between simulation and experiments were accounted for. However, the simulations demonstrated that the energy barrier for micelle rupture was significantly larger than what was calculated from the experimental force data in [34] and, unlike the experiments, the MD simulations showed the scission energy to be a non-monotonic function of the ratio of salt to surfactant.

The dynamics of the filament rupture were experimentally captured using a high-speed digital video camera [53]. An example is shown in Figure 3(a). Unlike capillary driven filament break-up instabilities, which has been observed to occur in weakly strain hardening fluids after considerable necking of the fluid filament [59], the failure of these wormlike micelle filaments occurs before any significant necking has occurred. The failure appears to be initiated by the growth of a surface or internal defect in the filament that rapidly propagates across the filament cleaving it in two. The propagation of the defect and final failure of the fluid filament is quite rapid, taking less time to complete than the break-up time of the wormlike micelles. A review of the dynamics of the necking of viscoelastic fluid filaments was presented by Renardy [60]. In his review, Renardy showed that the purely elastic instabilities that were observed in these filament stretching experiments are independent of surface tension and can occur for fluids in which the extensional viscosity goes through a maximum with increasing strain. The observed filament failure mechanism appears similar to failures observed in tensile loading of elastic solids and extremely elastic polymer melts [61-63]. For the case of elastic solids, samples experiencing a uniform tensile deformation become unstable and fail when the force or the engineering stress goes through a maximum [61]; the Considère criteria [64]. At that point, the solid has exhausted its work-hardening capacity and begun to work-soften, destabilizing any perturbation along the sample and producing a neck that grows rapidly with time.

As we will discuss in the following section, the failure of micelle solutions in uniaxial extensional flows has also been found to lead to new and interesting instabilities in more complex flows such as in the extensional flow in the wake of a sphere falling through a wormlike micelle solution and the flow of a wormlike micelle solution past a rigid or flexibly mounted cylinder. These instabilities have great significance to industrial flows of wormlike micelle solutions such as in turbulent drag reduction where strong extensional flow and flows with complex mixed kinematics are often encountered.

Perhaps the simplest way to study a complex flow is to apply a known pre-shear to a wormlike micelle solution just prior to stretching it in a FiSER. Bhardwaj *et al.* [36] studied the effect of pre-shear on extensional deformation of a number of CTAB/NaSal and CPyCl/NaSal wormlike micelle solutions. As the strength and duration of the applied shear rate were increased prior to a filament stretching experiment, the strain hardening of the extensional viscosity was delayed to larger Hencky strains. This trend is consistent with similar pre-shear measurements for polymer solutions [65], however, it should be noted that the delay is significantly more pronounced for wormlike micelles even at shear rates below a Weissenberg number of $Wi = \lambda \dot{\gamma} < 1$. The delay in strain hardening likely stems from the need for the micelle to either rotate from the shear direction where it was rotated during the pre-shear cycle into the stretch direction or, alternately, to compress back through its equilibrium conformation before it is subsequently stretched. In the no pre-shear case, the value of the elastic tensile stress at filament rupture was found to be independent of imposed extension rate, however, Bhardwaj *et al.* [36] found that the maximum elastic tensile stress and therefore the extensional viscosity decreased dramatically with increasing pre-shear rate and duration. The most dramatic effects were observed at shear rates for which shear banding had been observed, however,

the authors hypothesized that even in the absence of shear banding, the reduction in the strain hardening suggests that the pre-shear might reduce the size of the wormlike micelles or perhaps changes the interconnectivity of the micelle network prior to stretch. This is in stark contrast to the observations of Anna and McKinley [65] who observed no discernible difference in the steady-state value of the extensional viscosity of polymer solutions with and without pre-shear.

2.3 Capillary Break-up Extensional Rheometry

In a capillary break-up extensional rheometer (CaBER) shown in Figure 2(d), an initial nearly cylindrical fluid sample is placed between the two endplates of the filament stretching rheometer and stretched typically with an exponential profile, $L = L_0 \exp(\dot{\varepsilon}_0 t)$, to a final length of L_f . The stretch is then stopped and the capillary thinning of the liquid bridge formed between the two endplates produces a uniaxial extensional flow that can be used to measure an apparent extensional viscosity [66-71]. One of the advantages of the standard CaBER technique is that it is capable of measuring the extensional viscosity of fluids with shear viscosities as low as 70mPa·s and relaxation times as low as 10ms [66]. Furthermore, with the introduction of dripping on a substrate CaBER (CaBER-DoS) shown in Figure 2(e) [72, 73] solutions with shear viscosities on the order of water and relaxation times as small as 20 μ s are now measurable [74]. In addition, CaBER can reach extremely large Hencky strains, $\varepsilon > 10$, limited only by the resolution of the diameter measurement transducer or high-speed video camera.

The break-up of the fluid filament in CaBER device is driven by capillary stresses and resisted by the extensional stresses developed within the flow. The apparent extensional viscosity of the wormlike micelle solution can be determined by measuring the change in the filament diameter as a function of time. Papageorgiou [75] showed that for a Newtonian fluid the radius of the fluid filament will decay linearly with time in the absence of inertia, $R_{mid}(t) \propto (t_b - t)$. Conversely, Entov and Hinch [70] showed that for an Oldroyd-B model, the radius will decay exponentially with time, $R_{mid}(t) \propto \exp(-t/3\lambda_E)$ resulting in a flow with a constant extensional Weissenberg number of $Wi_E = \lambda_E \dot{\varepsilon} = 2/3$. This value is larger than the critical extensional Weissenberg number of $Wi_E = 1/2$ needed to achieve coil-stretch transition and thus strain hardening of the extensional viscosity of the wormlike micelle solutions can be achieved. Additionally, the slope of the diameter as a function of time can be used to calculate a relaxation time in this elongational flow, λ_E . Theoretical predictions assert that there should be no difference between the relaxation time measured in shear and extensional flow $\lambda_E \approx \lambda$ [70] although this is not necessarily observed in practice. This is likely do to the very rapid and poorly controlled step-strain required to produce the initial fluid filament [76]. An apparent extensional viscosity can be calculated by applying a force balance between capillary stresses and the elastic tensile stresses within the fluid filament [47]

$$\eta_{E,app} = \frac{\sigma / R_{mid}(t)}{\dot{\varepsilon}(t)} = \frac{-\sigma}{dD_{mid} / dt}.$$
 (2)

To calculate the extensional viscosity, the diameter measurements can either be numerically differentiated or fit with the functional form and then differentiated [67].

In Anderson *et al.* [39] and Yesilata *et al.* [38], a capillary break-up extensional rheometer was used to measure the extensional viscosity of erucyl bis(hydroxyethyl)methylammonium chloride (EHAC) and iso-proponal in a brine of ammonium chloride in deionized water. Their results showed a strong extensional hardening for all of the surfactant and salt concentrations that they tested. Additionally, Yesilata *et al.* [38]

demonstrated that the extensional relaxation time, λ_E , extracted from intermediate decay of the fluid filament for the EHAC solutions was smaller by approximately a factor of three than the longest relaxation time obtained from oscillatory shear flow measurements, λ . This observation is different from capillary break-up measurements of Boger fluids where the relaxation times were found to be approximately equal, $\lambda_E \approx \lambda$, as expected from theory [67]. Later CaBER measurements by Bhardwaj et al. [35] for a series of CPyCl/NaSal and CTAB/NaSal wormlike micelle solutions showed that the ratio of the extensional relaxation time to the shear relaxation time, λ_E/λ , started at a value much less than one and increased monotonically with increasing surfactant concentration to a value greater than one. Additionally, Miller [77] demonstrated that the value of the extensional relaxation time measured was a strong function of the extension rate and total strain imposed on the fluid filament during the initial step-stretch. Finally, if one compares the extensional viscosity measured in CaBER to that in FiSER at nominally the same extension rate, the results do not always agree. Bhardwaj et al. [35] showed that for CPyCl/NaSal solutions, the extensional viscosity measurements from FiSER are in some instances more than an order of magnitude larger than those measured using CaBER. These results demonstrate the sensitivity of these self-assembling wormlike micelle solutions to the precise dynamics of the extensional flow and suggest that caution should be used when interpreting CaBER measurements of the extensional viscosity of wormlike micelle solutions and other self-assembling systems.

Interesting recent extensional rheology measurements have suggested that the response of the micelles with different microstructure (branched or linear) is different in uniaxial extensional flows and therefore, extensional flows are sensitive to the type of micellar microstructures. A systematic study of the role of branching on the extensional rheology of wormlike micelles was performed by Chellamuthu and Rothstein [37] using both a filament stretching extensional rheometer and capillary break-up extensional rheometer. The experiments were performed using a series of linear and branched wormlike micelle solutions consisting of octyltrimethylammonium bromide and sodium oleate, C₈TAB/NaOA. Both the shear and extensional viscosity of wormlike micelle solutions were found to demonstrate a maximum in viscosity

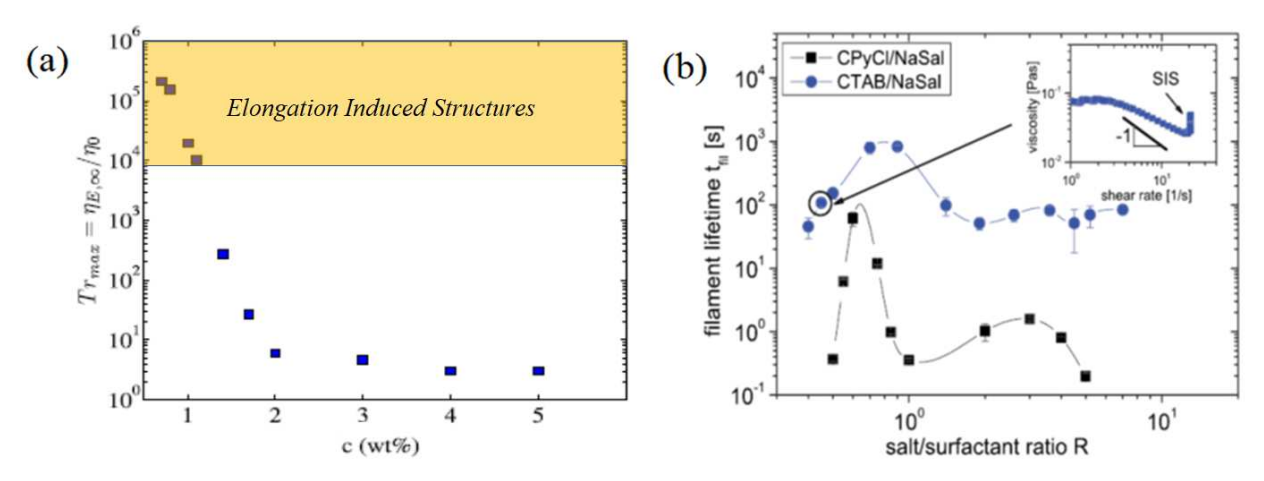


Figure 4: Extensional rheology results from CaBER measurements of linear and branched wormlike micelle solutions. In (a), the maximum Trouton ratio is presented as a function of concentration of CTAT in water [22]. A transition from linear to unbranched highly dense was observed at 2wt%. In (b), the filament lifetime is shown as a function of ratio of salt to surfacetant for CPyCl/NaSal and CTAB/NaSal solutions to highlight the formation of shear induced and extension induced structure (EIS) in the wormlike micelle solutions [40].

at total surfactant concentration of 4wt%. For these systems, the steady-state value of the Trouton ratio was found to decay monotonically and rapidly with increasing micelle concentration, approaching an asymptote close to the Newtonian limit for concentrations of 4wt% and above. Through cryo-TEM imaging, this maximum in the shear viscosity has been shown to be the result of a transition from linear to branched micelles [18, 78, 79]. Chellamuthu and Rothstein [37] hypothesized that the dramatic loss of extensional viscosity like that shown in Figure 4(a) coincided with the onset of branching and was most likely due to the additional stress relief mechanisms via 'ghost-like' crossing of micelles at entanglement points with increasing surfactant concentration and the presence of branches. This of course is very different from the response of polymer solutions where branching is known to increase the strain hardening of the extensional viscosity. These authors suggest that the lack of strain hardening of the extensional viscosity could be an indicator of the presence of branching [22, 37].

More recently, Omidvar et al. [22] investigated the extensional rheology of micellar solutions based on cetyltrimethylammonium tosylate (CTAT) in water over a range of concentrations (0.7 wt% - 5 wt%). Their data is shown in Figure 4(a). Beyond concentration of 2 wt%, a maximum in shear relaxation time was observed and linked to a transition from linear wormlike micelles to unbranched and short wormlike micelles via cryo-TEM imaging. Omidvar et al. [22] showed that by increasing the concentration of surfactant the maximum Trouton ratio decreases and beyond the critical concentration of 2wt%, Trouton ratio reaches an asymptotic value close to Tr = 3; a result that is similar to Chellamuthu and Rothstein [37]

More recent results of the group of Willenbacher [40] has investigated the effect of branching on extensional rheology of CTAB/NaSal and CPyCl/NaSal systems using CaBER by systematically varying the ration of salt to surfactant, R. Their measurements presented in Figure 4(b) showed that solutions of linear and branched micelles could be distinguished by differences in how the lifetime of the filament in CaBER scaled with shear viscosity. For linear systems, they found that $t_{fil} \propto \eta_0^{1.3}$ while branched systems scaled with $t_{fil} \propto \eta_0^{0.9}$. Similar differences in the filament lifetime scaling with zero shear rate viscosity were observed by Omidvar et al. [80] on CPyCl/NaSal systems that show a linear to branched transition with increasing salt concentration, but saw no difference in the scaling of filament lifetime for $C_8TAB/NaOA$ system which showed a transition from a linear to unbranched and short wormlike micelles with increasing salt concentration. In addition, Omidvar et al. [80] compared the extensional rheological results of CaBER with the CaBER-DOS and showed that both the maximum Trouton ratio and extensional relaxation times measured by the CaBER are consistently lower than those of measured with the CaBER-DOS device. These authors have attributed this difference to extensional flow-induced micellar breakage that are more likely occur in CaBER experiments due to large initial perturbation imposed to wormlike micelles.

More interestingly, Sachsenheimer et al. [40] showed for the CTAB systems specifically, that at low values of R, where micellar solutions exhibit shear thickening as shown in Figure 4(b), strong evidence of Extensional Flow-Induced Structure (EIS) was present in the data. EIS was characterized by formation of long filament lifetime in dilute micellar solutions as shown in Figure 4(b) and has been linked to flow-induced aggregation of rod-like isolated micelles to giant wormlike aggregates. Sachsenheimer et al. [40] argued that the large Trouton ratios observed by Chellamuthu and Rothstein [37] might be the result of EIS in their systems as well. This would also explain the incredibly large Trouton ratios measured for the dilute CTAT micelle solutions. Omidvar et al. [22] showed that the Trouton ratio was $Tr > 10^5$ at a concentration of c = 0.7wt%. Using the asymptotic analysis of the FENE-P model, Omidvar et al. [22] estimated the final

length of the micelles during extensional flow measurements and showed that it is much higher (by orders of magnitude) than the equilibrium micellar length for this system [22]. More recently, Recktenwald et al. [81] performed particle image velocimetry on the extensional flow of a dilute micellar solution based on CTAB/NaSal and showed that EIS is accompanied by a heterogenous flow field. Finally, the presence of EIS has also been seen in complex flows with mixed kinematics. In the flow of a CTAB/NaSal solution into a contraction-expansion, Hashimoto et al. [82] observed turbidity along the centerline upstream of the contraction where the extensional flow is the strongest and argued that this turbidity was evidence of EIS.

Finally, recent introduction of the CaBER-DoS device has enabled extensional flow measurements in dilute complex fluids [72-74, 83]. However, it has been recently demonstrated by Wu and Mohammadigoushki [84], that the presence of the free contact-line on the lower substrate of the CaBER-DoS may strongly affect the reliable measurements of the extensional rheological properties of the complex fluids, specifically that of the wormlike micelles. Therefore, in performing CaBER-DoS experiments, it may be necessary to pin the fluid contact-line using a small lower substrate, which allows for the fluid contact-line to be pinned over the course of filament thinning process.

The ability to characterize the shear and extensional rheology of the wormlike micelle solutions makes it possible to better understand and perhaps even predict the response of these fluids to more complicated flow fields. In the following sections, we will explore a number of complex flows of wormlike micelle solutions where a wealth of interesting new dynamics have been observed over the last few years and go into some depth into a number of important applications of these materials where the fluids experience complex flows.

3. FLOW AROUND A FALLING SPHERE

Over the last 20 years, a number of research groups have examined the flow of the self-assembled surfactant solutions past a falling sphere [53, 85-93]. Historically, the first study was reported in 2003 by Jayaraman and Belmonte [85] who examined sedimentation of a sphere in a shear-banding wormlike micellar fluid based on 9mM/9mM solution of CTAB/NaSal [85]. These authors demonstrated that beyond a critical shear Weissenberg number of Wi > 45, the falling sphere experiences an instability that is characterized by sudden fluctuations in sphere sedimentation velocity. An example of unsteady sphere sedimentation is shown in Figure 5(a) and 5(b). Here, the Weissenberg number Wi is defined with the shear rate as $Wi = \lambda \dot{\gamma}$ where the characteristic shear rate is defined as $\dot{\gamma} = U/d$, where U is the average sphere sedimentation velocity and d is the sphere diameter. Jayaraman and Belmonte hypothesized that this instability in sphere sedimentation velocity or the fluid instability in the wake of the sphere (henceforth referred to as wake instability) is linked to the shear banding phenomenon [85]. Around almost the same time, Chen and Rothstein reported similar instabilities for a falling sphere in a shear banding wormlike micelles based on CTAB/ NaSal (50 mM/50 mM), for $Wi \ge 4$ [53]. These researchers showed that for conditions that give rise to wake instability, the filament of the wormlike micelles undergoes a sudden rupture in the FiSER experiments [53] as described above in Section 2.2. They therefore concluded that the wake instability is directly linked to the flow-induced micellar chain scission.

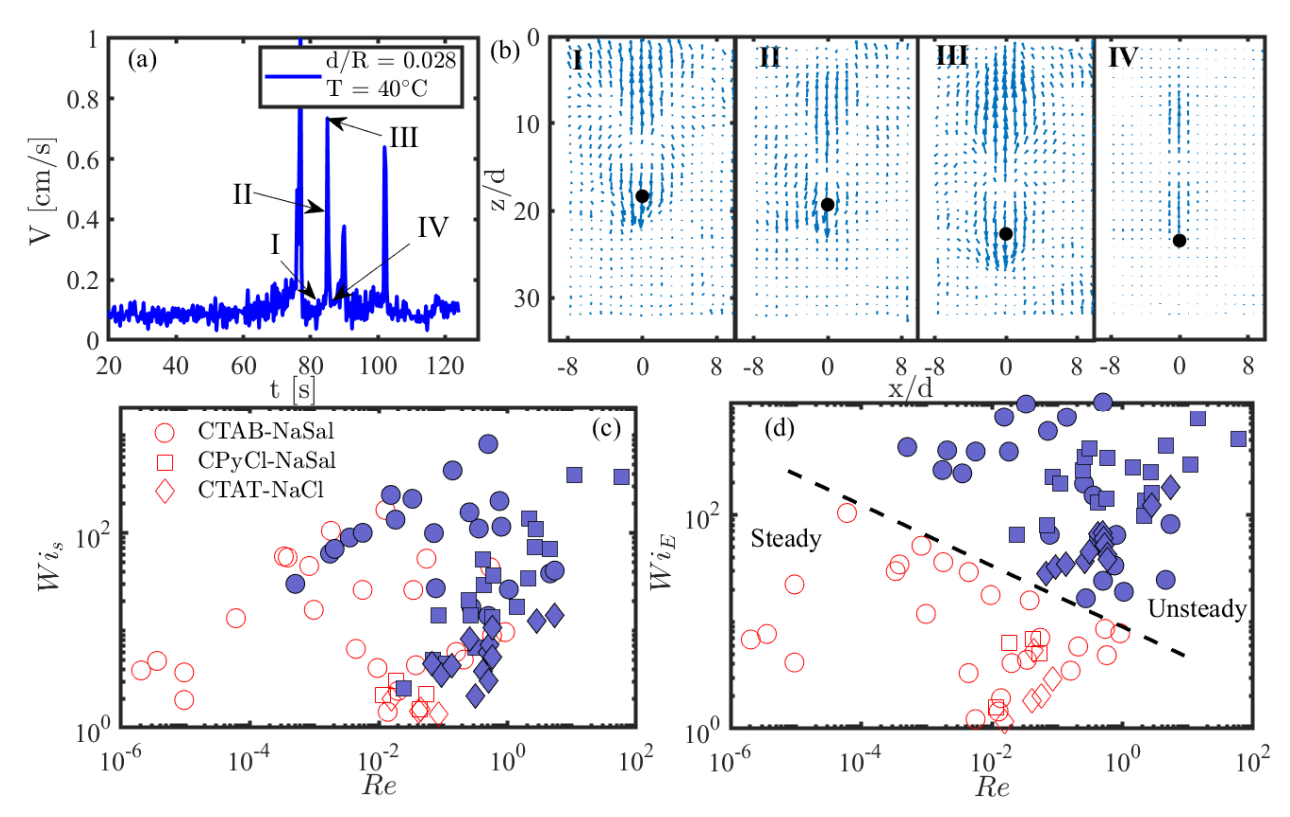


Figure 5. (a) Temporal evolution of velocity of the sphere center of mass depicting the acceleration, deceleration moment. (b) Instantaneous velocity vectors around a sedimenting sphere at the moment of instability. (c) Weissenberg number as a function of Reynolds number for sphere sedimentation experiments in a host of wormlike micellar fluids. (d) Extensional Weissenberg number as a function of Reynolds for similar experiments shown in part (c) [88].

More recently, Mohammadigoushki and Muller [88] carried out a systematic sphere sedimentation study using several different compositions of wormlike micellar solutions based on CTAB/NaSal over a wide range of temperature and flow rate conditions resulting in sedimentation experiments that varied between $1 \le Wi \le 10^3$ and $10^{-6} \le Re \le 10$. A phase diagram of sedimentation stability was initially produced using the characteristic shear conditions, Wi-Re, as shown in Figure 5(c). Unfortunately, using these criteria the data for steady and unsteady sedimentation could not be separated from each other. The authors then used PIV to probe the velocity field in the wake of the sphere and calculated the maximum local extension rate, $\dot{\varepsilon}_{\text{max}}$, in order to generate an extensional Weissenberg number, $Wi_E = \lambda \dot{\varepsilon}_{\text{max}}$, for each case as shown in Figure 5(d). By replotting the phase diagram using the extension conditions, Wie-Re, Mohammadigoushki and Muller [88] were able to successfully distinguish steady from unsteady sphere sedimentation experiments. They showed that the critical Weissenberg number for the onset of unsteady sedimentation decreased with increasing Reynolds number suggesting that inertia aids in the breakdown of wormlike micelles. Moreover, Zhang and Muller [92], carried out similar sphere sedimentation experiments in CTAT/NaCl and CPyCl/NaSal systems and confirmed that the criterion based on the extensional Weissenberg number can distinguish steady from unsteady sphere sedimentation experiments. These results, taken together, provide strong evidence that the wake instability in the wormlike micelles is linked to the scission of the wormlike chains in the wake of the falling sphere, where a strong extensional flow is present. Moreover, Zhang et al. [94] showed that the wake instability can occur for both shear banding and

non-shear banding wormlike micelles. They, therefore argued that this instability is not related to shear banding as originally argued by Jayaraman and Belmonte [85].

Although the wake instability in flow past a falling sphere has been consistently seen in wormlike micellar solutions, it is worth mentioning that a similar wake instability has been documented in viscoelastic polymer solutions [95, 96]. For example, Bisgaard [95] reported oscillations in the axial velocity in the flow behind a falling sphere in viscoelastic solutions through experiments at high shear Weissenberg numbers $Wi \sim 30$ and negligible inertia. Additionally, similar fluctuating behaviour was observed in experiments by Mollinger et al. [97] in a viscoelastic solution based on guar gum. Binous and Phillips [96] also reported similar instabilities in numerical simulations of a suspension of non-interacting FENE dumbbells past a falling sphere and linked that to formation of the gradients in the dumbbell extension on the flanks of the sphere. Moreover, Graessley and Milner [98] studied start-up of simple shear flow of viscoelastic polymer solutions using a multi-mode Maxwell model. They calculated the transient evolution of velocity profile upon inception of a step shear flow inside the gap of a parallel plate geometry and illustrated that for a solution with a single relaxation time, the fluctuations in fluid velocity persists for long times (typically t > 30 λ) after inception of the start-up of a shear flow, while for polymer solutions with a broad spectrum of relaxation times, oscillations disappear in a short period of time ($t \sim 3\lambda$). Wormlike micelles share many similarities with polymer solutions, therefore, it is conceivable that similar phenomena (i.e., gradient in micellar extensions around the falling sphere and the micellar relaxation spectrum) could control the wake instability in wormlike micellar solutions. This prompted Wu and Mohammadigoushki [90] to examine the effects of these two parameters on wake instability in wormlike micellar solutions. By studying two model micellar solutions, one with a single relaxation and the other with a broad relaxation spectrum, these authors showed that, indeed the micellar relaxation spectrum significantly affect the wake instability such that in highly entangled wormlike micelles with a broad spectrum of relaxation times, the instability never occurs, while in single mode Maxwell fluids the wake instability prevails. In addition, Wu and Mohammadigoushki [90] used flow induced birefringence to measure the micellar extension on the flanks of the falling spheres and illustrated that for cases that lead to wake instability no gradients in micellar extension exist.

It is very well-known that wormlike micellar solutions exhibit strong wall-slip at a moving solid boundary in simple shear flows [99-109]. Therefore, it is likely that the wall-slip phenomenon may affect the sphere sedimentation dynamics in micellar solutions. Mohammadigoushki and Muller [89] studied the role of sphere boundary condition on the sphere sedimentation dynamics in wormlike micellar solutions of CTAB/NaSal (9mM/9mM) and showed that a roughened sphere sediments faster than a smooth (unroughened) sphere in this wormlike micellar solution. This was due to presence of small micron-sized bubbles that form at the sphere surface and enhance the wall-slip. Following their removal from the sphere surface, the sphere sedimentation velocity for roughened and smooth spheres were similar [89].

Thus far, studies on flow of the surfactant solutions past a falling sphere have mainly focused on the semi-dilute concentration regime in which long, entangled and flexible wormlike micelles exist. Wu and Mohammadigoushki [91] have examined the problem of sphere sedimentation in dilute micellar solutions that exhibit shear thickening. These researchers demonstrated that at a vanishingly small Reynolds number, the drag coefficient for the falling sphere in a dilute micellar solution was similar to that of a Newtonian fluid. Surprisingly, however, for conditions that correspond to 0.09 < Re < 9.86, falling spheres experienced a significant drag reduction. Moreover, an unusually extended wake which spans over an incredible distance of $L_{wake} > 80d$ downstream of the sphere was detected by particle image velocimetry. These unusual results were linked to formation of extensional flow-induced structure as described previously in Section 2.3. Due to the strong shear and/or extensional flows around the falling sphere, micelles could aggregate into giant

wormlike structures. The authors argued that the presence of giant wormlike micelles may induce significant sphere drag reduction while simultaneously extended elastic wakes in the rear of sphere [91].

4. FLOW AROUND A CIRCULAR CYLINDER

Fluid flow around a circular cylinder in cross-flow of a non-Newtonian fluid is a canonical problem that has been the subject of number of both experimental [110-120] and numerical studies [119, 121-123] primarily for the flow of polymer solutions. Only recently has the flow of wormlike micelle solutions past a circular cylinder been investigated [124-129]. Moss and Rothstein [124, 125] studied flow of two different micelle solutions past a single circular cylinder and an array of circular cylinders. They used a 50mM/50mM CTAB/NaSal solution in water as well as a 100mM/50mM CPyCl/NaSal solution in 50mM NaCl salt solution. Pressure drop measurements showed a constant normalized pressure drop until a shear Weissenberg number of approximately $Wi = \lambda \dot{\gamma} = 1$. For Weissenberg numbers between $1 \le Wi \le 4$, the normalized pressure drop decreases with increasing Weissenberg number due to the shear thinning of the micelle solutions. At larger Weissenberg numbers, a broad plateau was reached, before the pressure drop began to increase again for $Wi \ge 7$ for the CPyCl/NaSal. The latter result was linked to strain hardening of the micelle solution. From FiSER measurements the CPyCl/NaSal solution was found to strain harden reaching a Trouton ratio of well over Tr > 100. The pressure drop did not increase for the CTAB/NaSal solution. Unlike the CPyCl/NaSal solution, which was found to be stable over all Weissenberg numbers tested, the flow of the CTAB/NaSal solution above $Wi \ge 4.5$ was found to become unstable.

To determine the origin of the flow instability, Moss and Rothstein [124, 125] employed particle image velocimetry (PIV) and flow induced birefringence (FIB) measurements. The PIV measurements demonstrated large velocity gradients around the equator of the cylinders and strong extensional flow downstream of the cylinders. Examples of both FIB and PIV measurements from Haward et al. [88] is shown in Figure 6. At high flow rates, a long birefringent tail downstream of the cylinder was observed by the FIB, highlighting the elongation of the micelles in the extensionally dominated flow in the cylinder's wake.

Beyond a Weissenberg number of Wi > 4.5, the PIV and FIB measurements of the CTAB/NaSal solution were found to become time dependent. By studying the FIB in the wake of the cylinder, it was observed that at a critical stress, the fluid appeared to tear in the wake of the cylinder. The result is a sudden acceleration of the fluid, a break in the vertical symmetry, and a reduction in the number of fringes. At that time, much of the resistance to flow is lost and the fluid accelerates around the cylinder as the tail appears to oscillate back and forth with time. As the Weissenberg number was increased, the rupture events were observed to occur more frequently. Moss and Rothstein [124, 125] showed that difference in the stability of the CTAB/NaSal and the CPyCl/NaSal solutions could be understood by analysing the rupture events that occurred during FiSER experiments. In FiSER, at extensional Weissenberg numbers similar to those calculated from the local PIV measurements in the wake of the cylinder, CTAB/NaSal filaments were observed to rupture after an extensional Hencky strain of $\varepsilon = 2.4$ was accumulated while the CPyCl/NaSal filaments failed at $\varepsilon = 3.3$. As a result, the CPyCl/NaSal solutions remained stable even at high Weissenberg numbers because, in the wake of the cylinder, an extensional strain of just $\varepsilon = 2.5$ was accumulated. The

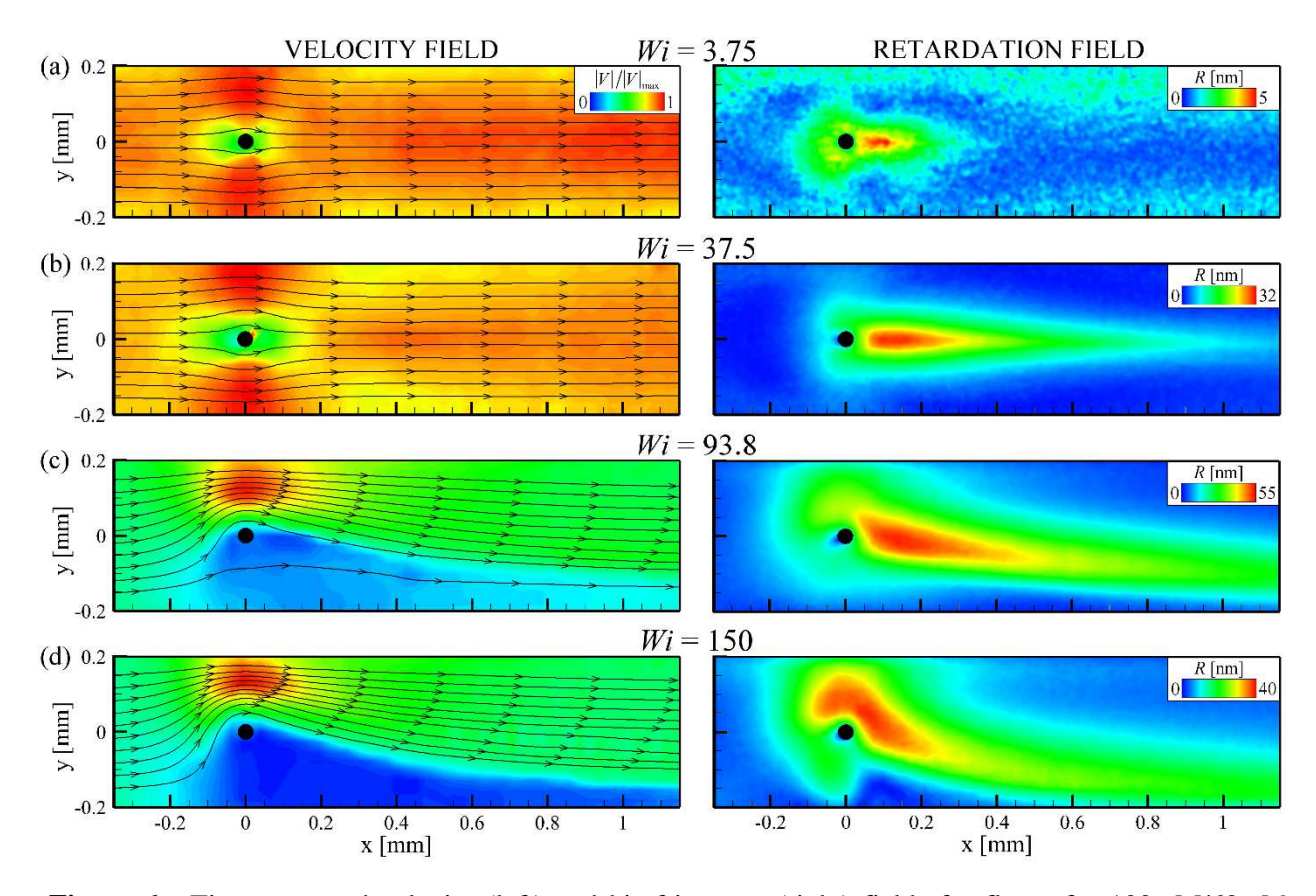


Figure 6: Time averaged velocity (left) and birefringence (right) fields for flow of a 100 mM/60 mM CPCl/NaSal wormlike micelle solution flowing past a cylinder [128]. The flow shows marked asymmetry beyond Wi > 60 and becomes unsteady beyond Wi > 130.

extensional rheology measurements therefore suggest that only the CTAB/NaSal micelles should rupture in the wake of the cylinder to induce an elastic flow instability.

Haward et al. [128] investigated the flow of a 100mM CPyCl and 60mM NaSal aqueous wormlike micelle solution past a microfluidic circular cylinder shown in Figure 6. They used a novel glass fabrication process to fabricate high aspect ratio, H/W = 5, and low blockage ratio, d/W = 0.1, circular cylinders. Here H is the height of the channel and W is its width, while d is the diameter of the cylinder. This is quite different from typical PDMS-based microfluidic devices where it is challenging to fabricate cylinders with aspect ratios much bigger than one. Due to the small diameter of the cylinder, Haward et al. [128] were able to probe shear Weissenberg numbers significantly larger than those explored previously studied, Wi < 3750, while still maintaining a vanishingly small Reynolds number. Through detailed PIV and FIB measurements, they demonstrated two distinct flow transitions. The first occurred at approximately Wi = 60 and was characterized by a strong asymmetry in the flow with the fluid taking a preferred path around one side of the cylinder. In some cases, the asymmetry was so stark that flow was observed to stagnate on one side of the cylinder. With increased Weissenberg number beyond Wi > 130, the flow was found to become time transient through an elastic instability that is consistent with the observations of Moss and Rothstein [124, 125]. This flow asymmetry had been seen previously by Dey et al. [126] for the flow of a CTAB/NaSal solution past a flexible cylinder. Haward et al. [130] recently showed that this asymmetry can also be observed with a polymer solution and that its observation requires both strong shear thinning of the shear viscosity and significant strain hardening of the extensional viscosity.

Recent theoretical predictions of flow around a circular cylinder have been performed by Khan and Sasmal [131]. In their simulations, they used the Vasquez, Cook and McKinley (VCM) model to describe the wormlike micelle solutions. The VCM model is based on kinetic theory that can account for the breakage and reformation of micelles. In this model, micelle breakage depends on the local rate of deformation and the breakage rate specified for the micelles. When subjected to flow, a chain can break into two smaller chains of equal length. These small chains can then recombine with time to form a longer chain of length *L*. The VCM model has been shown to correctly predict transient and steady shear banding [109, 132] and extensional thickening [133] in wormlike micellar solutions. The simulations of Khan and Sasmal [131] showed an elastic flow instability similar to that observed in the experiments at a critical Weissenberg number. Interestingly, they showed that as the wormlike micelle solution get easier to break, that the elastic flow instability can be delayed to higher Weissenberg numbers or even completely eliminated. This observations may help explain some of the large differences that have been observed in the critical Weissenberg number for the onset of elastic instabilities as the concentration or type of surfactant and salt are changed from one experiment to the next.

4.1 Viscoelastic Fluid Structure Interactions (VFSI)

The elastic flow instability observed for the flow of wormlike micelles solutions past rigid circular cylinders was used by Dey et al. [126, 127, 134, 135] as the driving force needed to excite motion of both flexible and flexibly-mounted cylinders and sheets. Their experiments opened up a new field of study called Viscoelastic Fluid Structure Interactions (VFSI) and inspired the work of other research groups including Hopkins et al. [129]. In Dey et al. [126], a 50mM CTAB and 25mM NaSal aqueous wormlike micelle solution was used. A soft PDMS cylinder with an elastic modulus of 0.5MPa was placed across the flow. The deformation and motion of the cylinder was tracked with time along with PIV and FIB measurements. Beyond a shear Weissenberg number of Wi > 106, the flow became unstable and the cylinder began to oscillate as shown in Figure 7. The frequency of oscillation began at f = 0.2Hz or roughly $f = 1/\lambda$ and increased linearly with increasing Weissenberg number. The amplitude of oscillation was found to initially increase before reaching a maximum and decaying with increasing Weissenberg number. Unlike the oscillation pattern observed for Newtonian FSI which results from the shedding of vortices downstream of the cylinder and are sinusoidal in nature, the oscillation patterns observed had a saw tooth profile shown in Figure 7 resulting from the slow growth of elastic stress in the extensional wake of the cylinder and the sudden, violent release of the elastic stress upon the breakdown of the wormlike micelles in the wake of the cylinder. Beyond a second critical Weissenberg number of Wi > 223, the oscillations of the cylinder went from a 1D oscillation purely in the flow direction to 2D oscillation where the cylinder traced out an elliptical pattern that was both in the flow and transverse direction. In a later study, Dey et al. [127] showed that if the frequency of vortex shedding matched

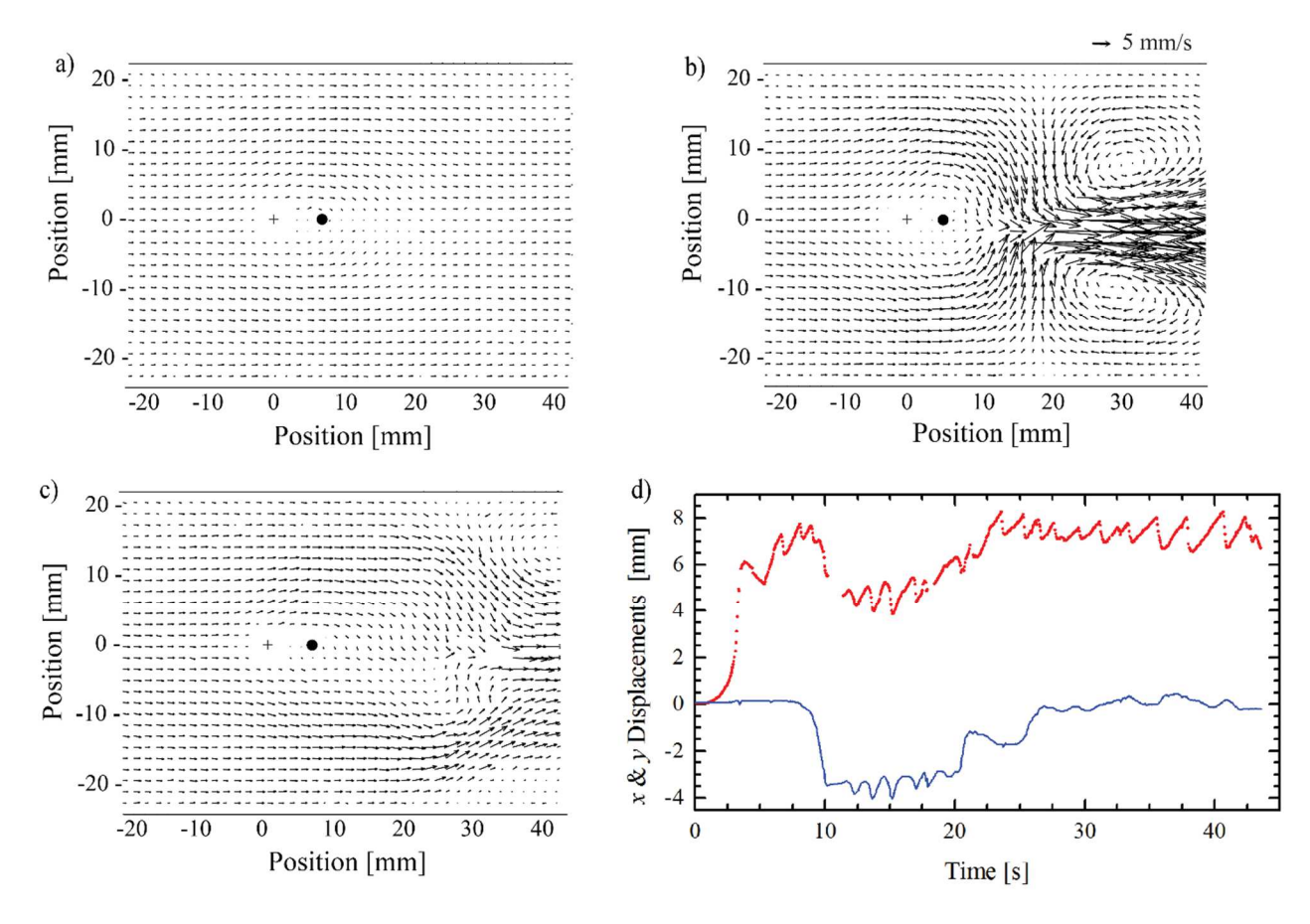


Figure 7: PIV vector fields showing the unstable flow of wormlike micelle solution around a flexible cylinder at Wi = 280 [126]. The images in a) and b) are t = 0.12s while b) and c) are 0.06s apart. The unstable flow leads to an oscillatory motion of the flexible cylinder in both x (upper curve) and y (lower curve) shown in d) for Wi = 390.

the natural frequency of the cylinder, then a two-way coupling could be observed and a region of lock-in akin to the behavior observed in Newtonian FSI was found. In this lock-in region, the frequency of oscillation remained fixed at the natural frequency of the flexibly mounted cylinder while the amplitude of oscillation grew monotonically with Weissenberg number even beyond the lock-in regime. This lock-in behavior is quite different from that observed for Newtonian fluids.

VFSI has also been observed in microfluidic devices. Hopkins et al. [129] redesigned the microfluidic glass circular cylinders described in Haward et al. [128] so that they were cantilevered from one side of the flow cell while leaving a small gap between the free end and the wall flow cell. They showed that the elastic flow instabilities at the microscale were strong enough to produce significant oscillations. They extended the work from a single cylinder to two cylinders aligned along the center of the microchannel but spaced more than ten diameters, 10D, apart and found a strong coupling between the two cantilevered cylinders as they were found to beat in time with near perfect synchrony even when the observed oscillations were 2D in nature.

5. FLOW THROUGH OTHER COMPLEX GEOMETRIES

Flow of wormlike micelles in complex geometries have focused primarily on cross-slot, contraction-expansion and 90° degree bend. The common feature of these geometries is that micellar solutions experience a combination of both extension, shear deformation and/or stream-line curvature.

5.1 Contraction Expansion

Experimental studies on the contraction-expansion geometry have mainly focused on either axisymmetric or planar flows. Hashimoto et al. [82] studied flow of wormlike micellar solutions of CTAB/NaSal at various salt to surfactant concentration ratios in a 11:1 axisymmetric contraction geometry and reported four flow regimes including: 1) a Newtonian response at low flow rates, 2) formation of stable vortices in the salient corner of the contraction that increase in size by increasing the imposed flow rate, 3) temporally fluctuating vortices and 4) turbulence. Like the observations of Dey et al. [126, 134] for flow past cylinders and sheets, the oscillations in the pressure drop through the contraction-expansion in regime 3 were observed to have a saw tooth profile [82] and not the typical sinusoidal profile observed for the flow of polymer solutions through contraction-expansions [136]. In addition, Hashimoto et al. [82] observed formation of a highly orientated wormlike micellar solution at the entrance of the contraction and attributed that to the extensional flow induced micellar orientation. More recently, Salipante et al. [137] studied flow of a series of wormlike micellar solutions in an axisymmetric gradual contraction, and a sudden contraction with a contraction ratio of approximately 8:1. These authors observed a transition from stable to unstable asymmetric flow beyond a critical extensional Weissenberg number around $Wi_E \sim 10$ and linked that to the breakdown of the micellar microstructure (or extensional flow induced micellar breakage) [137].

In addition to axisymmetric geometry, flow transitions have been documented in planar contraction-expansions. For example, Matos et al. [138] observed three flow regimes upon increasing the imposed shear rates in wormlike micellar solutions of CTAB/NaSal and CPyCl/NaSal; a Newtonian-like pattern at low imposed shear rates, which transitions to formation of two asymmetric fluctuating vortices in the salient corners and finally to a chaotic and highly time dependent flow pattern at high shear rates. Lutz-Bueno et al. [139] reported similar transitions for a highly elastic wormlike micellar solution based on 10mM/10mM CTAB/NaSal. Interestingly, Lutz-Bueno et al. [139] illustrated that as the imposed flow rate is increased, the size of the vortices is decreased; a result that is different from experiments of Hashimoto et al. [82] in an axisymmetric contraction-expansion. Finally, by utilizing a time-averaged SANS experiments, Lutz-Bueno et al. [139] illustrated that close to the side-walls of the flow geometry, micelles were not stretched, while, at the center-line of the contraction, micelles were highly-stretched and aligned in the direction of the flow.

Theoretical studies of the flow of wormlike micellar solutions in planar contraction-expansion geometries have mainly used three models including, molecular dynamics (MD) simulations, the modified Bautista-Manero (MBM) and the Vasquez-Cook-McKinley (VCM) models discussed previously. In studying the non-linear flows of wormlike micelles, Manero et al. [140] developed the Bautista-Manero model whereby stress is described by the Oldroyd-B constitutive equations and the viscosity is given by a kinetic model that consists of terms for construction and destruction of micelles. The MBM model is a modified version of the original BM model proposed to resolve the issues associated with the unbounded response during extensional thickening [141].

Stukan and co-workers [142-145] have used molecular dynamic (MD) simulations to model response of wormlike micelles including their dynamic length, density and orientation in contraction-expansion

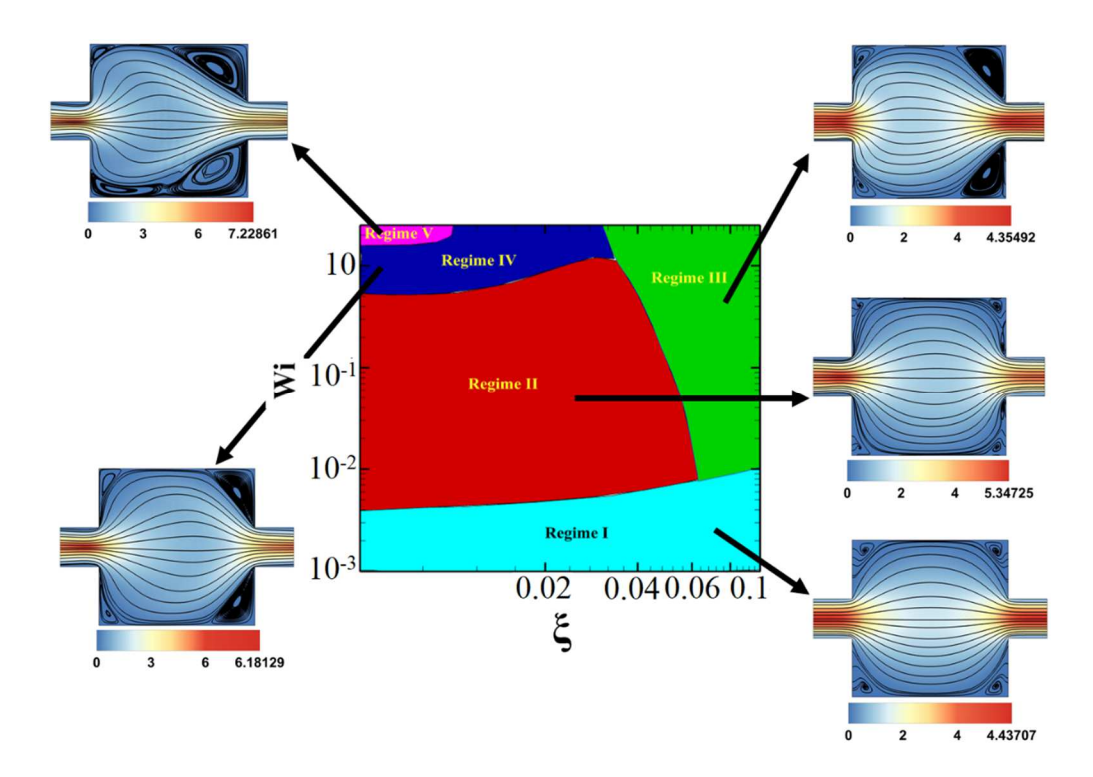


Figure 8. A phase diagram that illustrates different possible regimes in simulation of the VCM model as a function of Weissenberg number and the rate of micellar breakage [147].

flows. These MD simulations require knowledge of the background flow field. For a Newtonian background flow and a contraction similar in size to the radius of gyration of the micelles, MD simulations show no change in the micellar length and breakage/reformation events inside the simulating domain [142], while for a non-Newtonian background flow (measured directly by the particle image velocimetry [145]) and a geometry much larger than the micelle size, micellar length and breakage/reformation were strongly non-uniform at high Deborah numbers, $De \sim 1$. Here the Deborah number is defined as $De = \lambda / t_c$ where t_c is the characteristic time of the flow defined by the authors as the time for the micelles to complete a single pass through the simulation volume [143, 144]. On the other hand, simulations of the MBM model indicated that the extent of extensional thickening can significantly affect the flow of wormlike micelles in a 4:1 planar contraction flow. For moderately extensional hardening fluid parameters, the size of the vortex was shown to increase as a function of Weissenberg number up to a $Wi \sim 1$, while a sharp decrease was reported for Wi > 1. Whereas, for highly extensional hardening fluid, the size of the vortex was shown to decrease as a function of Wi followed by an increase beyond Wi > 10. Since most of wormlike micellar solutions are highly extensional hardening, the results of MBM model appear to be consistent with the experimental findings of Lutz-Bueno et al. [139]. Finally, Cromer and Cook [146] studied the flow behaviour of the VCM model in a slowly varying converging-diverging channel and showed that below the onset of shear thinning, the flow response is similar to that of a Newtonian fluid, while beyond the shear thinning regime, the flow is no longer fore-aft symmetric with flow localization forming near the maximum velocity gradients. More recently, Sasmal [147] presented an extensive numerical simulations of the VCM model in a planar contraction-expansion geometry by systematically varying the Weissenberg number and the VCM breakage/reformation parameter, ξ . Five different regimes were observed, which can be distinguished on a phase diagram based on Wi- ξ as shown in Figure 8. In regime I, at low Weissenberg numbers and all values of ξ , weak vortices formed in the salient corners of the geometry and the flow field was symmetric; a result that is similar to flow of Newtonian fluids. In regime II, in addition to salient vortices, lip vortices formed at both the entrant of the expansion and re-entrant to the contraction part of the flow field. In regime III, the lip vortex disappeared and the salient corner vortex grew in size. In regime IV, the corner vortices merged and formed a much larger corner vortex. In regime V, the flow became unsteady and temporal fluctuations were reported. While many of these predictions by the VCM and the MBM model remain to be tested in experiments, we note that one of the advantages of these models compared to the MD simulations is that the flow field need not to be known a priori. In fact, the resulting flow field is calculated in the simulations of the VCM and MBM models.

5.2 Cross Slot

Another microfluidic geometry that has received considerable attention is the cross-slot geometry. A cross slot consists of perpendicular channels with opposing inlets and opposing outlets at 90° to the inlets. Near the walls of the cross-slot channels, the flow is predominantly shear, while closer to the stagnation point, the extensional flow becomes prominent. The first study of the flow of wormlike micellar solutions in a cross-slot geometry is reported by Pathak and Hudson on CTAB/NaSal and on CPyCl/NaSal solutions [148]. These authors reported presence of bright birefringent bands in the vicinity of the stagnation point and noted an asymmetric flow due to the high elasticity of the wormlike micelles. Haward et al. [149] reported three flow regimes for flow of CPyCl/NaSal solutions in a microfluidic cross-slot geometry. At low Weissenberg numbers, the flow remained steady and symmetric. For Weissenberg numbers beyond Wi > 1, a steady asymmetric flow was developed. For Wi > 350, the flow was observed to fluctuate and was aperiodic. In addition, a lip vortex along the walls of the cross-slot geometry was observed in experiments by Haward et al. [149]. A similar study was reported by Haward and McKinley [150] who showed that the critical thresholds for these flow transitions in CPyCl/NaSal/NaCl system strongly depend on the surfactant concentrations and ionic strength. Dubash et al. [151] found flow transitions similar to those of Haward and co-workers [150] and observed formation of lip vortices at the corners of the microfluidic geometry. In addition, Dubash et al. [151] showed that the development of the lip vortex occurred before the onset of asymmetric flow for one fluid and after asymmetric flow onset for a different solution.

Although there have been several high-quality experimental studies on flow of viscoelastic wormlike micellar solutions in the cross-slot flow geometry, the theoretical studies on this flow system are limited. Recently Cromer and co-workers [152, 153] have started simulating the flow behaviour of wormlike micellar solutions in a cross-slot geometry using the VCM model. These authors showed that by increasing the flow rate, a transition from steady symmetric flow to an unsteady asymmetric flow is observed. In addition, a lip vortex along the walls of the inlets was observed and shown to increase in size as the flow rate increases; a result that yet to be verified in cross-slot experiments. Cromer and co-workers showed that breakage and reformation rates are needed for formation of the lip vortex and argued that the unstable flow is driven by micellar stretching and micellar breakage acts as a stabilizer for the elastic instability [153]. The latter results have also been reported in simulations of Sasmal [147] in the contraction-expansion flow geometry.

5.3 Sharp Bend

In addition to cross-slot geometry, and contraction-expansion flows, formation of secondary flows in flow of wormlike micelles has been documented in sharp 90° bend microfluidic devices, where strong stream-line curvatures are present [94, 154]. Hwang et al. [154] investigated flow of two wormlike micellar solutions based on the CPyCl/NaSal in a microfluid bend device via direct flow visualization as shown in Figure 9. By varying the salt to surfactant concentration, R, these authors formulated two wormlike micelles (R = 0.55); a viscoelastic micellar solution with linear morphology and R = 0.79; a branched shear-banding micellar solution). For the linear micellar solution, two flow transitions were reported as the imposed flow rate increased. The first transition was characterized by formation of a steady lip vortex upstream of the bend corner, which increased in size with increasing flow rate and the second transition was characterized by fluctuations in the size of the lip vortex with time. The increase of the vortex length with increasing flow rate is consistent with findings of Cromer and co-workers in cross-slot geometry [152, 153]. On the other hand, the branched micelles showed two distinctly different transitions. The first transition was characterized by the formation of a lip vortex and a vortex at the far corner of the bend. The second transition was characterized by the disappearance of the far corner and the onset of time fluctuations in the size of the lip vortex. Based on this study, the difference in flow patterns of these two wormlike micellar solutions was hypothesized to be due to either shear banding phenomenon or the differences in the micellar microstructure. To examine which factor has caused such a difference in flow patterns, Zhang et al. [94], formulated four set of wormlike micellar solutions; linear non-shear banding, linear shear banding, branched non-shear banding and a branched shear banding system. These authors reported no difference

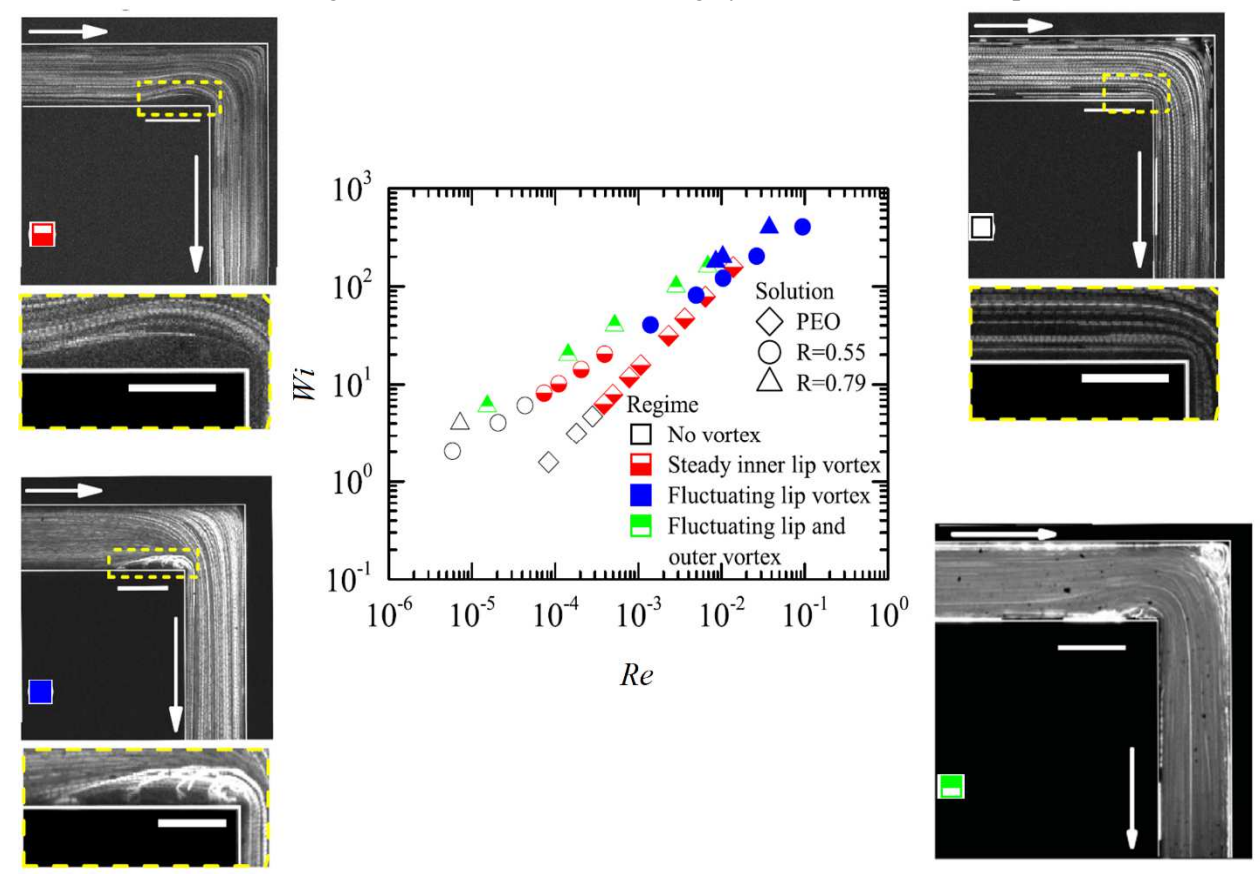


Figure 9. A phase diagram based on Weissenberg number as a function of Reynolds number for flows of wormlike micellar solutions and a polymer solution based on PEO through a microfluidic sharp-bend device. Snapshots showing different possible flow patterns for wormlike micellar fluids [154]. The snapshot that illustrates the fluctuating lip and outer vortex corresponds to the wormlike micelles with R = 0.79 and the rest of snapshots correspond to flow of wormlike micelles with R = 0.55.

between the non-shear banding linear and non-shear banding branched micelles in terms of flow transitions and therefore, concluded that the type of micellar microstructure plays a minimal role in these flow transitions. However, by comparing the shear banding with non-shear banding wormlike micelles at a fixed micellar morphology (linear or branched), they observed a significant difference in terms of flow transitions. As a result, they concluded that the differences in transitions reported in Hwang et al. [154] study are linked to shear banding phenomenon. It is worth noting that simulations of the wormlike micellar flows in sharp microfluidic bend devices are not available.

6. CONCLUSIONS AND OUTLOOK

We have reviewed the experimental and theoretical literature on complex flows of wormlike micelles, in which a combination of shear and extensional deformation exists. Although wormlike micelles have been studied for quite sometimes, their response in complex flows still remains enriched due to a strong positive feedback loop between the flow and the microstructure. Flow changes the microstructure of the wormlike micelles, and the microstructural changes affect the resulting stress field, and gradients in the stress field change the flow. This positive feedback loop holds the key in a more in-depth understanding of some of the important aspects of the flow including the critical thresholds for the onset of instabilities, and the form and the nature of the secondary flows in various complex geometries.

The microstructure of the micelles is controlled by various factors including the rate of the micellar breakage and reformation, the charged interaction between micelles, surfactant chemistry, surfactant concentration (dilute, semidilute, concentrated, nematic and hexagonal) and salt concentrations (linear micelles vs. branched micelles). Perhaps the most pressing questions on the complex flows of the micellar solutions are how micellar solutions with various topologies and chemistries react to complex flows? And, whether a universal criterion can be brought to bear to explain the onset of instability in complex flows of micellar solutions with various topologies and chemistries. i.e., Is it possible to lump all microstructural factors into one critical threshold for the onset of instability? How should one define the critical threshold for the onset of instability in complex flows of micellar solutions? Complex flows involve a combination of shear and extensional deformation. Therefore, defining the critical threshold based on the shear or extensional deformation is a subtle task. On the microscale, it is highly valuable to develop time-resolved microstructural based analysis techniques (e.g., SANS or SAXS) to elucidate the microscale response of the micelles in complex flows.

Majority of complex flow studies have thus far focused on semi-dilute concentrated regime. How does a dilute or a concentrated micellar solution (in the vicinity of zero-shear isotropic to nematic phase transition) behave in complex flows? Could flow-induced structuration in dilute regime and/or isotropic to nematic transition in concentrated micellar solutions modify the flow response and lead to new physics? Recent CaBER and porous medium experiments on dilute micellar solutions have shown interesting physics that arise from flow-induced structure formation under strong extensional flows, many aspects of which are still unknown [155]. At high surfactant/salt concentrations, wormlike micelles exhibit a gel-like behaviour [156, 157]. How does the yield stress manifest itself in complex flows of wormlike micelles?

Last but not least, further theoretical studies using physically relevant models such as VCM, MBM or other models that account for the effects of micellar breakage in complex flows could potentially help explain some of the existing experimental observations in complex flows.

ACKNOWLEDGEMENTS

The authors would like to express his sincere thanks to both their current and former students whose work constituted a large part of this review article. The authors would also like to thank the National Science Foundation (CBET CAREER 1942150 for HM and CBET-1705251 for JPR) for financial support.

REFERENCES

- [1] V.J. Anderson, J.R.A. Pearson, E.S. Boek, The Rheology of Worm-Like Micellar Fluids, in: D.M. Binding, K. Walters (Eds.) Rheology Reviews, The British Society of Rheology, 2006, pp. 217-253.
- [2] J.L. Zakin, H.W. Bewersdorff, Surfactant drag reduction, Rev. Chem. Eng., 14 (1998) 253-320.
- [3] C.A. Dreiss, Wormlike micelles: where do we stand? Recent developments, linear rheology and scattering techniques, Soft Matter, 3 (2007) 956-970.
- [4] M.E. Cates, S.M. Fielding, Rheology of giant micelles, Adv. Phys., 55 (2006) 799-879.
- [5] J. Yang, Viscoelastic wormlike micelles and their applications, Current Opinion in Colloid and Interface Sci., 7 (2002) 276-281.
- [6] S.A. Rogers, M.A. Calabrese, N.J. Wagner, Rheology of branched wormlike micelles, Curr. Opin. Colloid Interface Sci., 19 (2014) 530-535.
- [7] Y. Zhao, P. Cheung, A.Q. Shen, Microfluidic flows of wormlike micellar solutions, Adv. Coll. Int. Sci., 211 (2014) 34-46.
- [8] S. Lerouge, J.-F. Berret, Shear-Induced Transitions and Instabilities in Surfactant Wormlike Micelles, in: K. Dusek, J.-F. Joanny (Eds.) Advances in Polymer Science, Springer, New York, 2010, pp. 1-71.
- [9] J.N. Israelachvili, Intermolecular and surface forces: with applications to colloidal and biological systems, Academic Press, London, 1985.
- [10] R.G. Larson, The Structure and Rheology of Complex Fluids, Oxford University Press, New York, 1999.
- [11] H. Rehage, H. Hoffmann, Viscoelastic surfactant solutions: model systems for rheological research, Mol. Phys., 74 (1991) 933-973.
- [12] P. Schurtenberger, R. Scartazzini, L.J. Magid, M.E. Leser, P.l. Luisi, Structural and dynamic properties of polymer-like reverse micelles J. Phys. Chem., 94 (1990) 3695-3701.
- [13] S.-H. Tung, Y.-E. Huang, S.R. Raghavan, A new reverse wormlike micellar system: Mixtures of bile salt and lecithin in organic liquids, J. Am. Chem. Soc., 128 (2006) 5751-5756.
- [14] R.G. Laughlin, The Aqueous Phase Behavior of Surfactants, Academic Press, New York, 1994.
- [15] J.N. Israelachvili, Intermolecular and surface forces, 2nd ed., Academic Press, London; San Diego, 1992.
- [16] F. Lequeux, S.J. Candau, Structural Properties of Wormlike Micelles, in: T. McLeish (Ed.) Theoretical Challenges in the Dynamics of Complex Fluids, Kluwer Academic Publishers, Netherlands, 1997, pp. 181-190.
- [17] D. Danino, A. Bernheim-Groswasser, Y. Talmon, Digital cryogenic transmission electron microscopy: an advanced tool for direct imaging of complex fluids, Colloids and Surfaces A: Physicochemical and Engineering Aspects, 183 (2001) 113-122.
- [18] H. Cui, T.K. Hodgdon, E.W. Kaler, L. Abezgauz, D. Danino, M. Lubovsky, Y. Talmon, D.J. Pochan, Elucidating the assembled structure of amphiphiles in solution via cryogenic transmission electron microscopy, Soft Matter, 3 (2007) 945 955.
- [19] D. Danino, Y. Talmon, H. Levy, G. Beinert, R. Zana, Branched threadlike micelles in an aqueous solution of a trimeric surfactant, Science, 269 (1995) 1420-1421.
- [20] D. Danino, Y. Talmon, R. Zana, Alkanediyl-alpha,omega-bis(dimethylalkylammonium bromide) surfactants (dimeric surfactants). 5. Aggregation and microstructure in aqueous solutions, Langmuir, 11 (1995) 1448-1456.
- [21] D. Danino, Y. Talmon, R. Zana, Cryo-TEM of thread-like micelles: on-the-grid microstructural transformations induced during specimen preparation, Colloids and Surfaces A: Physiochemical and Engineering Aspects, 169 (2000) 67-73.
- [22] R. Omidvar, A. Dalili, A. Mir, H. Mohammadigoushki, Exploring sensitivity of the extensional flow to wormlike micellar structure, J. Non-Newt. Fluid Mech., 252 (2018) 48-56.
- [23] J. Appell, G. Porte, A. Khatory, F. Kern, S.J. Candau, Static and dynamic properties of a network of wormlike surfactant micelles (etylpyridinium chlorate in sodium chlorate brine), J. Phys. II, 2 (1992) 1045-1052.
- [24] S. Kefi, J. Lee, T. Pope, P. Sullivan, E. Nelson, A. Hernandez, T. Olsen, M. Parlar, B. Powers, A. Roy, A. Wilson, A. Twynam, Expanding applications for viscoelastic surfactants, Oilfield Review, (2004) 10-16.

- [25] G.H. McKinley, T. Sridhar, Filament stretching rheometry, Annu. Rev. Fluid Mech., 34 (2002) 375-415.
- [26] R.K. Prud'homme, G.G. Warr, Elongational flow of solutions of rodlike micelles, Langmuir, 10 (1994) 3419-3426.
- [27] C. Chen, G.G. Warr, Light scattering from wormlike micelles in an elongational flow, Langmuir, 13 (1997) 1374-1376.
- [28] P. Fischer, G.G. Fuller, Z. Lin, Branched viscoelastic surfactant solutions and their responses to elongational flow, Rheol. Acta, 36 (1997) 632-638.
- [29] B. Lu, X. Li, L.E. Scriven, H.T. Davis, Y. Talmon, J.L. Zakin, Effect of chemical structure on viscoelasticity and extensional viscosity of drag-reducing cationic surfactant solutions, Langmuir, 14 (1998) 8-16.
- [30] L.M. Walker, P. Moldenaers, J.-F. Berret, Macroscopic response of wormlike micelles to elongational flow, Langmuir, 12 (1996) 6309-6314.
- [31] M. Kato, T. Takahashi, M. Shirakashi, Steady planar elongational viscosity of CTAB/NaSal aqueous solutions measured in a 4-roll mill flow cell, J. Soc. Rheol. Jpn., 30 (2002) 283-287.
- [32] M. Kato, T. Takahashi, M. Shirakashi, Flow-induced structure change and flow instability of CTAB/NaSal aqueous solution in 4-roll mill flow cell, in: Int. Congr. on Rheol., Seoul, Korea, 2004, pp. FE20-21-23.
- [33] A.J. Muller, M.F. Torres, A.E. Saez, Effect of the flow field on the rheological behavior of aqueous cetyltrimethylammonium *p*-toluenesulfonate solutions, Langmuir, 20 (2004) 3838-3841.
- [34] J.P. Rothstein, Transient extensional rheology of wormlike micelle solutions, J. Rheol., 47 (2003) 1227-1247.
- [35] A. Bhardwaj, E. Miller, J.P. Rothstein, Filament stretching and capillary breakup extensional rheometry measurements of viscoelastic wormlike micelle solutions, J. Rheol., 51 (2007) 693-719.
- [36] A. Bhardwaj, D. Richter, M. Chellamuthu, J.P. Rothstein, The effect of preshear on the extensional rheology of wormlike micelle solutions, Rheol. Acta, 46 (2007) 861-875.
- [37] M. Chellamuthu, J.P. Rothstein, Distinguishing between linear and branched wormlike micelle solutions using extensional rheology measurements, J. Rheol., 52 (2008) 865-884.
- [38] B. Yesilata, C. Clasen, G.H. McKinley, Nonlinear shear and extensional flow dynamics of wormlike surfactant solutions, J. Non-Newtonian Fluid Mech., 133 (2006) 73-90.
- [39] V.J. Anderson, P.M.J. Tardy, J.P. Crawshaw, G.C. Maitland, Extensional flow of wormlike micellar fluids, in: Int. Congr. Rheol., Seoul, Korea, 2004, pp. FE07-01-03.
- [40] D. Sachsenheimer, C. Oelschlaeger, S. Muller, J. Kustner, S. Bindgen, N. Willenbacher, Elongational deformation of wormlike micellar solutions, J. Rheol., 58 (2014) 2017–2042.
- [41] G.G. Fuller, C.A. Cathey, B. Hubbard, B.E. Zebrowski, Extensional viscosity measurements for low-viscosity fluids, J. Rheol., 31 (1987) 235-249.
- [42] P.K. Bhattacharjee, J. Oberhauser, G.H. McKinley, L.G. Leal, T. Sridhar, Extensional rheometry of entangled solutions, Macromol., 35 (2002) 10131-10148.
- [43] Y. Hu, S.Q. Wang, A.M. Jamieson, Elongational Flow Behavior of Cetyltrimethylammonium Bromide/Sodium Salicylate Surfactant Solutions, J. Phys. Chem., 98 (1994) 8555-8559.
- [44] Z.Q. Lin, B. Lu, J.L. Zakin, Y. Talmon, Y. Zheng, H.T. Davis, L.E. Scriven, Influence of surfactant concentration and counterion to surfactant ratio on rheology of wormlike micelles, J. Colloid and Interface Sci., 239 (2001) 543-554.
- [45] T.J. Ober, S.J. Haward, C.J. Pipe, J. Soulages, G.H. McKinley, Microfluidic Extensional Rheometry using a Hyperbolic Contraction Geometry, Rheol Acta, 52 (2013) 529-546.
- [46] B.F. Garcia, S. Saraji, Mixed in-situ rheology of viscoelastic surfactant solutions using a hyperbolic geometry, J Non-Newton Fluid, 270 (2019) 56-65.
- [47] S.L. Anna, G.H. McKinley, D.A. Nguyen, T. Sridhar, S.J. Muller, J. Huang, D.F. James, An inter-laboratory comparison of measurements from filament stretching rheometers using common test fluids, J. Rheol., 45 (2001) 83-114.
- [48] V. Tirtaatmadja, T. Sridhar, A filament stretching device for measurement of extensional viscosity, J. Rheol., 37 (1993) 1133-1160.
- [49] P. Szabo, Transient filament stretching rheometry I: Force balance analysis, Rheol. Acta, 36 (1997) 277-284.
- [50] P. Szabo, G.H. McKinley, Filament stretching rheometer: Inertia compensation revisited, Rheol. Acta, 42 (2003) 269-272.
- [51] L.E. Wedgewood, D.N. Ostrov, R.B. Bird, A finite extensible bead-spring chain model for dilute polymer-solutions, J. Non-Newtonian Fluid Mech., 40 (1991) 119-139.
- [52] T. Shikata, S.J. Dahman, D.S. Pearson, Rheo-optic behavior of wormlike micelles, Langmuir, 10 (1994) 3470-3476.

- [53] S. Chen, J.P. Rothstein, Flow of a wormlike micelle solution past a falling sphere, J. Non-Newtonian Fluid Mech., 116 (2004) 205-234.
- [54] L.B. Smolka, A. Belmonte, Drop pinch-off and filament dynamics of wormlike micellar fluids, J. Non-Newtonian Fluid Mech., 115 (2003) 1-25.
- [55] Q. Huang, O. Hassager, Polymer liquids fracture like solids, Soft Matter, 13 (2017) 3470--3474.
- [56] S. Dhakal, R. Sureshkumar, Topology, length scales, and energetics of surfactant micelles, J. Chem. Phys., 143 (2015) 024905.
- [57] S. Dhakal, R. Sureshkumar, Uniaxial Extension of Surfactant Micelles: Counterion Mediated Chain Stiffening and a Mechanism of Rupture by Flow-Induced Energy Redistribution, ACS Macro Lett., 5 (2016) 108–111.
- [58] T. Mandal, R.G. Larson, Stretch and Breakage of Wormlike Micelles under Uniaxial Strain: A Simulation Study and Comparison with Experimental Results, Langmuir, 34 (2018) 12600-12608.
- [59] M. Yao, G.H. McKinley, B. Debbaut, Extensional deformation, stress relaxation and necking failure of viscoelastic filaments, J. Non-Newtonian Fluid Mech., 79 (1998) 469-501.
- [60] M. Renardy, Self-similar breakup of non-Newtonian fluid jets, in: D.M. Binding, K. Walters (Eds.) Rheology Reviews, The British Society of Rheology, Aberystwyth, UK, 2004, pp. 171-196.
- [61] T.H. Courtney, Mechanical Behavior of Materials, McGraw Hill, Boston, 2000.
- [62] Y.M. Joshi, M.M. Denn, Rupture of entangled polymeric liquids in elongational flows, J. Rheol., 47 (2003) 291-298.
- [63] G.V. Vinogradov, A.Y. Malkin, V.V. Volosevitch, V.P. Shatalov, V.P. Yudin, Flow, high-elastic (recoverable) deformations and rupture of uncured high molecular weight linear polymers in uniaxial extension, J. Poly. Sci. Polym. Phys. Ed., 13 (1975) 1721-1735.
- [64] G.H. McKinley, O. Hassager, The Considere condition and rapid stretching of linear and branched polymer melts, J. Rheol., 43 (1999) 1195-1212.
- [65] S.L. Anna, G.H. McKinley, Effect of a controlled pre-deformation history on extensional viscosity, Rheol. Acta, 47 (2008) 841-859.
- [66] L.E. Rodd, T.P. Scott, J.J. Cooper-White, G.H. McKinley, Capillary break-up rheometry of low-viscosity elastic fluids, Appl. Rheol., 15 (2005) 12-27.
- [67] S.L. Anna, G.H. McKinley, Elasto-capillary thinning and breakup of model elastic liquids, J. Rheol., 45 (2001) 115-138.
- [68] G.H. McKinley, A. Tripathi, How to extract the Newtonian viscosity from capilary breakup measurements in a filament rheometer, J. Rheol., 44 (2000) 653-670.
- [69] M. Stelter, G. Brenn, A.L. Yarin, R.P. Singh, F. Durst, Validation and application of a novel elongational device for polymer solutions, J. Rheol., 44 (2000) 595-616.
- [70] V.M. Entov, E.J. Hinch, Effect of a spectrum of relaxation times on the capillary thinning of a filament of elastic liquid, J. Non-Newtonian Fluid Mech., 72 (1997) 31-53.
- [71] A.V. Bazilevsky, V.M. Entov, A.N. Rozhkov, Liquid filament microrheometer and some of its applications, in: D.R. Oliver (Ed.) Proc. Third European Rheology Conference, Edinburgh, 1990, pp. 41-43.
- [72] J. Dinic, L.N. Jimenez, V. Sharma, Pinch-off dynamics and dripping-onto-substrate (DoS) rheometry of complex fluids, Lab Chip, 17 (2017) 460-473.
- [73] J. Dinic, Y. Zhang, L.N. Jimenez, V. Sharma, Extensional Relaxation Times of Dilute, Aqueous Polymer Solutions, ACS Macro Lett., 4 (2015) 804-808.
- [74] S. Sur, J.P. Rothstein, Drop breakup dynamics of dilute polymer solutions: Effect of molecular weight, concentration and viscosity J. Rheol., 62 (2018) 1245-1259.
- [75] D.T. Papageorgiou, On the breakup of viscous liquid threads, Phys. Fluids, 7 (1995) 1529-1544.
- [76] E. Miller, C. Clasen, J.P. Rothstein, The effect of step-stretch parameters on capillary breakup extensional rheology (CaBER) measurements, Rheol. Acta, 48 (2009) 625-639.
- [77] E. Miller, The Dynamics and Rheology of Shear-Banding Wormlike Micelles and Other Non-Newtonian Fluids, in: Mechanical Engineering, University of Massachusetts, Amherst, 2007.
- [78] L. Ziserman, Relationship between Rheological Properties and Nanostructure in Mixed Micellar Surfactant, in: Dept. Biotechnology and Food Engineering, Technion Israel Institute of Technology, 2005.
- [79] S.R. Raghavan, G. Fritz, E.W. Kaler, Wormlike micelles formed by synergistic self-assembly in mixtures of anionic and cationic surfactants, Langmuir, 18 (2002) 3797-3803.
- [80] R. Omidvar, S. Wu, H. Mohammadigoushki, Detecting wormlike micellar microstructure using extensional rheology, J. Rheol., 63 (2019) 33-44.
- [81] S.M. Recktenwald, S.J. Haward, A.Q. Shen, N. Willenbacher Heterogeneous flow inside threads of low viscosity fluids leads to anomalous long filament lifetimes, Scientific Reports, 9 (2019) 711.

- [82] T. Hashimoto, K. Kido, S. Kaki, T. Yamamoto, N. Mori, Effects of surfactant and salt concentrations on capillary flow and its entry flow for wormlike micelle solutions, Rheol. Acta, 45 (2006) 841-852.
- [83] M. Rosello, S. Sur, B. Barbet, J.P. Rothstein, Dripping-onto-substrate capillary breakup extensional rheometry of low viscosity printing inks, J. Non-Newt. Fluid Mech., 266 (2019) 160-170.
- [84] S. Wu, H. Mohammadigoushki, Effects of moving contact line on filament pinch-off dynamics of viscoelastic surfactant fluids, Phys. Rev. Fluids, 5 (2020) 053303.
- [85] A. Jayaraman, A. Belmonte, Oscillations of a solid sphere falling through a wormlike micellar fluid, Phys. Rev. E, 67 (2003) 065301.
- [86] N. Kumar, S. Majumdar, A. Sood, R. Govindarajan, S. Ramaswamy, A.K. Sood, Oscillatory settling in wormlike-micelle solutions: bursts and a long time scale, Soft Matter, 8 (2012) 4310.
- [87] M. Kostrzewa, A. Delgado, A. Wierschem, Particle settling in micellar solutions of varying concentration and salt content, Acta Mech., 227 (2016) 677.
- [88] H. Mohammadigoushki, S.J. Muller, Sedimentation of a sphere in wormlike micellar fluids, J. Rheol., 60 (2016) 587-601.
- [89] H. Mohammadigoushki, S.J. Muller, Creeping flow of a wormlike micelle solution past a falling sphere: Role of boundary conditions, J. Non-Newt. Fluid Mech., 257 (2018) 44-49.
- [90] S. Wu, H. Mohammadigoushki, Sphere sedimentation in wormlike micelles: Effect of micellar relaxation spectrum and gradients in micellar extensions, J. Rheol., 62 (2018) 1061-1069.
- [91] S. Wu, H. Mohammadigoushki, Flow of a model shear-thickening micellar fluid past a falling sphere, Phys. Rev. Fluids, 4 (2019) 073303.
- [92] Y. Zhang, S.J. Muller, Unsteady sedimentation of a sphere in wormlike micellar fluids, Phys. Rev. Fluids, 3 (2018) 043301.
- [93] Z. Wang, S. Wang, L. Xu, Y. Dou, X. Su, Extremely slow settling behavior of particles in dilute wormlike micellar fluid with broad spectrum of relaxation times, Journal of Dispersion Science and Technology, (2019) 1-9.
- [94] Y. Zhang, H. Mohammadigoushki, M.Y. Hwang, S.J. Muller, Flow of wormlike micellar fluids around a sharp bend: Effects of branching and shear-banding, Physical Review Fluids, 3 (2018) 093301.
- [95] C. Bisgaard, Velocity-fields around spheres and bubbles investigated by laser-Doppler anemometry, J. Non-Newtonian Fluid Mech., 12 (1983) 283-302.
- [96] H. Binous, R.J. Phillips, Dynamic simulation of one and two particles sedimenting in viscoelastic suspensions of FENE dumbbells., J Non-Newton Fluid, 83 (1999) 93-130.
- [97] A.M. Mollinger, E.C. Cornelissen, B.H.A.A. van den Brule, An unexpected phenomenon observed in particle settling: oscillating falling spheres, J. Non-Newtonian Fluid Mech., 86 (1999) 389-393.
- [98] W.W. Graessley, S.T. Milner, Inertially driven transient response in polymeric liquids, J. Non-Newtonian Fluid Mech., 159 (2009) 26-33.
- [99] M.A. Fardin, S. Lerouge, Instabilities in wormlike micelle systems, Eur. Phys. J. E (2012) 35: 91, 35 (2012) 91.
- [100] A. Mendez-Sanchez, J. Perez-Gonzalez, L. de Vargas, J.R. Castrejon-Pita, A.A. Castrejon-Pita, G. Huelsz, Particle image velocimetery of the unstable capillary flow of a micellar solutions, J. Rheol., 47 (2003) 1455-1466.
- [101] M.P. Lettinga, S. Manneville, Competition between Shear Banding and Wall Slip in Wormlike Micelles, Phys. Rev. Lett., 103 (2009) 248302.
- [102] L. Becu, S. Manneville, A. Colin, Spatiotemporal dynamics of wormlike micelles under shear, Physical Review Letters, 93 (2004) 018301.
- [103] Y.T. Hu, A. Lips, Kinetics and mechanism of shear banding in entangled micellar solutions, J. Rheol., 49(5) (2005) pp. 1101-1027.
- [104] M.R. Lopez-Gonzalez, W.M. Holmes, P.T. Callaghan, Rheo-nmr phenomena of wormlike micelles Soft Matter, Soft Matter, 2 (2006) 855–869.
- [105] R.W. Mair, P.T. Callaghan, Observation of shear banding in worm-like micelles by NMR velocity imaging, Europhys. Letters, 36 (1996) 719-724.
- [106] C. Masselon, J. Salmon, A. Colin, Nonlocal Effects in Flows of Wormlike Micellar Solutions, Phys. Rev. Lett., 100 (2008) 038301.
- [107] M.R. López-González, W.M. Holmes, P.T. Callaghan, P.J. Photinos, Shear Banding Fluctuations and Nematic Order in Wormlike Micelles, Phys. Rev. Lett., 93 (2004) 268302.
- [108] J.R. Brown, P.T. Callaghan, Changing micellar order, lever rule behavior and spatio-temporal dynamics in shear-banding at the onset of the stress plateau, Soft Matter, 7 (2011) 10472-10482.
- [109] H. Mohammadigoushki, A. Dalili, L. Zhou, P. Cook, Transient Evolution of Flow Profiles in a Shear Banding Wormlike Micellar Solution: Experimental Results and a Comparison with the VCM Model, Soft Matter, 15 (2019) 5483.

- [110] G.H. McKinley, R.C. Armstrong, R.A. Brown, The wake instability in viscoelastic flow past confined cylinders, Phil. Trans. Roy. Soc. London A, 344 (1993) 265-304.
- [111] C. Chmielewski, C.A. Petty, K. Jayaraman, Elastic instability in crossflow of polymer solutions through a periodic array of cylinders, J. Non-Newtonian Fluid Mech., 48 (1993) 285-301.
- [112] K.K. Talwar, B. Khomami, Flow of viscoelastic fluids past periodic square arrays of cylinders: inertial and shear thinning viscosity and elasticity effects, J. Non-Newtonian Fluid Mech., 57 (1995) 177-202.
- [113] F.P.T. Baaijens, S.H.A. Selen, H.P.W. Baaijens, G.W.M. Peters, H.E.H. Meijer, Viscoelastic flow past a confined cylinder of a low density polyethylene melt, J. Non-Newtonian Fluid Mech., 68 (1997) 173-203.
- [114] H.P.W. Baaijens, G.W.M. Peters, F.P.T. Baaijens, H.E.H. Meijer, Viscoelastic Flow Past a Confined Cylinder of a Polyisobutylene Solution, J. Rheol., 39 (1995) 1243-1277.
- [115] H. Usui, T. Shibata, Y. Sano, Karman Vortex Behind a Circular-Cylinder in Dilute Polymer-Solutions, J. Chem. Eng. Japan, 13 (1980) 77-79.
- [116] S.A. Dhahir, K. Walters, On Non-Newtonian Flow Past a Cylinder in a Confined Flow, J. Rheol., 33 (1989) 781-804.
- [117] J.M. Verhelst, F.T.M. Nieuwstadt, Visco-elastic flow past circular cylinders mounted in a channel: experimental measurements of velocity and drag, J. Non-Newtonian Fluid Mech., 116 (2004) 301-328.
- [118] S. Ogata, Y. Osano, K. Watanabe, Effect of Surfactant Solutions on the Drag and the Flow Pattern of a Circular Cylinder, AIChE J., 52 (2006) 49-57.
- [119] A.W. Liu, D.E. Bornside, R.C. Armstrong, R.A. Brown, Viscoelastic flow of polymer solutions around a periodic, linear array of cylinders: comparisons of predictions for microstructure and flow fields, J. Non-Newtonian Fluid Mech., 77 (1998) 153-190.
- [120] R.J. Marshall, A.B. Metzner, Flow of Viscoelastic Fluids through Porous Media, Industrial & Engineering Chemistry Fundamentals, 6 (1967) 393.
- [121] M.A. Hulsen, R. Fattal, R. Kupferman, Flow of viscoelastic fluids past a cylinder at high Weissenberg number: Stabilized simulations using matrix logarithms, J. Non-Newtonian Fluid Mech., 127 (2005) 27-39.
- [122] A. Liu, Viscoelastic Flow of Polymer Solutions Around Arrays of Cylinders: Comparison of Experiment and Theory, in: Chemical Engineering, MIT Dept. Chemical Engineering, Cambridge, 1997, pp. 330.
- [123] P.J. Oliveira, A.I.P. Miranda, A numerical study of steady and unsteady viscoelastic flow past bounded cylinders, J. Non-Newtonian Fluid Mech., 127 (2005) 51-66.
- [124] G.R. Moss, J.P. Rothstein, Flow of Viscoelastic Wormlike Micelle Solutions through a Periodic Array of Cylinders, J. Non-Newtonian Fluid Mech., 165 (2010) 1-13.
- [125] G.R. Moss, J.P. Rothstein, Flow of wormlike micelle solutions past a confined circular cylinder, J. Non-Newtonian Fluid Mech., 165 (2010) 1505-1515.
- [126] A.A. Dey, Y. Modarres-Sadeghi, J.P. Rothstein, Viscoelastic fluid-structure interactions between a flexible cylinder and wormlike micelle solution, Phys. Rev. Fluids, 3 (2018) 063301.
- [127] A. Dey, Y. Modarres-Sadeghi, J.P. Rothstein, Observation of lock-in for viscoelastic fluid-structure interactions, in press J. Fluids and Structures, (2020).
- [128] S.J. Haward, N. Kitajima, K. Toda-Peters, T. Takahashi, A.Q. Shen, Flow of wormlike micellar solutions around microfluidic cylinders with high aspect ratio and low blockage ratio†, Soft Matter, 15 (2019) 1927-1941.
- [129] C.C. Hopkins, S.J. Haward, A.Q. Shen, Purely Elastic Fluid-Structure Interactions in Microfluidics: Implications for Mucociliary Flows, Small, (2019) e1903872.
- [130] S.J. Haward, C.C. Hopkins, A.Q. Shen, Asymmetric flow of polymer solutions around microfluidic cylinders: Interaction between shear-thinning and viscoelasticity, in press J. Non-Newt. Fluid Mech., (2020).
- [131] M.B. Khan, C. Sasmal, Effect of chain scission on flow characteristics of wormlike micellar solutions past a confined microfluidic cylinder: a numerical analysis, Soft Matter, 16 (2020) 5261-5272.
- [132] C.J. Pipe, N.J. Kim, L.P. Cook, P.A. Vasquez, G.H. McKinley, Wormlike Micellar Solutions II: Comparison between experimental data and scission model predictions, J. Rheol., 54 (2010) 881-912.
- [133] M. Cromer, G.H. McKinley, L.P. Cook, Extensional flow of wormlike micellar solutions, Chem. Eng. Sci., 64 (2009) 4588-4596.
- [134] A.A. Dey, Y. Modarres-Sadeghi, J.P. Rothstein, Experimental Observation of Viscoelastic Fluid-Structure Interactions, J. Fluid Mech., 813 (2016) R5.
- [135] A. Dey, A. Lindner, Y. Modarres-Sadeghi, J.P. Rothstein, Oscillations of a cantilevered micro beam driven by a viscoelastic flow instability, Soft Matter, 16 (2020) 1227-1235.
- [136] J.P. Rothstein, G.H. McKinley, The axisymmetric contraction-expansion: The role of extensional rheology on vortex growth dynamics and the enhanced pressure drop, J. Non-Newtonian Fluid Mech., 98 (2001) 33-63.

- [137] P.F. Salipante, S.E. Meek, S.D. Hudson, Flow fluctuations in wormlike micelle fluids, Soft Matter, 14 (2018) 9020.
- [138] R.M. Matos, M.A. Alves, F.T. Pinho, Instabilities in micro-contraction flows of semi-dilute CTAB and CPyCl solutions: rheology and flow instabilities, Experiments in Fluids, 60 (2019) 145.
- [139] V. Lutz-Bueno, J. Kohlbrecher, P. Fischer, Micellar solutions in contraction slit-flow: Alignment mapped by SANS, J Non-Newton Fluid, 215 (2015) 8-18.
- [140] O. Manero, F. Bautista, J.F.A. Soltero, J.E. Puig, Dynamics of worm-like micelles: the Cox-Merz rule, J. Non-Newtonian Fluid Mech., 106 (2002) 1-15.
- [141] O. Manero, J.H. Perez-Lopez, J.I. Escalante, J.E. Puig, F. Bautista, A thermodynamic approach to rheology of complex fluids: The generalized BMP model, J. Non-Newt. Fluid Mech., 146 (2007) 22-29.
- [142] M.R. Stukan, E.S. Boek, J.T. Padding, W.J. Briels, J.P. Crawshaw, Flow of wormlike micelles in an expansion-contraction geometry, Soft Matter, 4 (2008).
- [143] J.P. Padding, W.J. Briels, M.R. Stukan, E.S. Boek, Review of multi-scale particulate simulation of the rheology of wormlike, Soft Matter, 5 (2009) 4367–4375.
- [144] M.R. Stukan, E.S. Boek, J.T. Padding, J.P. Crawshaw, Influence of system size and solvent flow on the distribution of wormlike micelles in a contraction-expansion geometry, Eur. Phys. J. E, 26 (2008) 63-71.
- [145] E.S. Boek, J.T. Padding, V.J. Anderson, W.J. Briels, J.P. Crawshaw, Flow of entangled wormlike micellar fluids: Mesoscopic simulations, rheology and μ -PIV experiments, J. Non-Newtonian Fluid Mech., 146 (2007) 11-21.
- [146] M. Cromer, L.P. Cook, A study of pressure-driven flow of wormlike micellar solutions through a converging/diverging channel, Journal of Rheology, 60 (2016) 953.
- [147] C. Sasmal, Flow of wormlike micellar solutions through a long micropore with step expansion and contraction, Phys. Fluids, 32 (2020) 013103.
- [148] J.A. Pathak, S.D. Hudson, Rheo-optics of Equilibrium Polymer Solutions: Wormlike Micelles in Elongational Flow in a Microfluidic Cross-Slot, Macromolecules, 39 (2006) 8782-8792.
- [149] S.J. Haward, T.J. Ober, M.S.N. Oliveira, M.A. Alves, G.H. McKinley, Extensional rheology and elastic instabilities of a wormlike micellar solution in a microfluidic cross-slot device, Soft Matter, 8 (2012) 536-555.
- [150] S.J. Haward, G.H. McKinley, Stagnation point flow of wormlike micellar solutions in a microfluidic cross-slot device: Effects of surfactant concentration and ionic environment, Phys Rev E, 85 (2012) 031502.
- [151] N. Dubash, P. Cheung, A.Q. Shen, Elastic instabilities in a microfluidic cross-slot flow of wormlike micellar solutions wormlike micellar solutions, Soft Matter, 8 (2012) 5845-5856.
- [152] A. Kalb, L.A. Villasmil-Urdaneta, M. Cromer, Role of chain scission in cross-slot flow of wormlike micellar solutions, Physical Review Fluids, 2 (2017) 071301(R).
- [153] A. Kalb, L.A. Villasmil-Urdaneta, M. Cromer, Elastic instability and secondary flow in cross-slot flow of wormlike micellar solutions, J Non-Newton Fluid, 262 (2018) 79-91.
- [154] M.Y. Hwang, H. Mohammadigoushki, S.J. Muller, Flow of viscoelastic fluids around a sharp microfluidic bend: Role of wormlike micellar structure, Phys. Rev. Fluids, 2 (2017) 043303.
- [155] M. Vasudevan, E. Buse, D. Lu, H. Krishna, A. Shen, B. Khomami, R. Sureshkumar, Irreversible nanogel formation in surfactant solutions by microporous flow, Nature Materials, 9 (2010) 436-441.
- [156] S.R. Raghavan, E.W. Kaler, Highly Viscoelastic Wormlike Micellar Solutions Formed by Cationic Surfactants with Long Unsaturated Tails, Langmuir, 17 (2001) 300-306.
- [157] W.-J. Kim, S.-M. Yang, Effects of Sodium Salicylate on the Microstructure of an Aqueous Micellar Solution and Its Rheological Responses, J. Colloid and Interface Sci., 232 (2000) 225-234.